

Article

Electron Probe Microanalysis and Microscopy of Polishing-Exposed Solid-Phase Mineral Inclusions in Fuxian Kimberlite Diamonds

Donggao Zhao 

Electron Microscope Laboratory of School of Dentistry, Department of Earth and Environmental Sciences, University of Missouri-Kansas City, Kansas City, MO 64108, USA; zhaodo@umkc.edu

Abstract: Solid-phase mineral inclusions in diamond (1–3 mm in diameter) from the No. 50 kimberlite diatreme of Liaoning Province, China, were exposed by polishing. A variety of silicate, carbonate and sulfide inclusions were recovered in the diamond. The common solid-phase inclusions are olivine, chromite, garnet and orthopyroxene; the rare phases include Ca carbonate, magnesite, dolomite, norsethite, pyrrhotite, pentlandite, troilite, a member of the linnaeite group, an unknown hydrous magnesium silicate and an Fe-rich phase. Abundance and composition of the solid-phase inclusions in diamond indicate that they belong to the peridotitic suite and are mainly harzburgitic. No eclogitic mineral inclusions were found in the diamond. The slightly lower Mg # of the olivine inclusions (peak at 93) than that of harzburgitic olivine inclusions worldwide (Mg # peak at 94), the higher Ni content (0.25–0.45 wt. %) of the olivine inclusions than those of olivine inclusions worldwide (0.30–0.40 wt. %), the higher Ti contents (up to 0.79 wt. %) in some chromite inclusions in diamond than those in chromite inclusions worldwide, the existence of carbonate inclusions in diamond, and the possible presence of hydrous silicate phases in diamond all indicate a metasomatic enrichment event in the source region of diamond beneath the North China craton, suggesting that the diamond probably formed by solid-state growth under metasomatic conditions with the presence of a fluid. Solid-state growth of diamond is also supported by abundant graphite inclusions in the diamond. Sulfide inclusions in diamond often coexist with chromite and olivine or are rich in Ni content, indicating that the sulfide inclusions belong to the peridotitic suite. From the chemical compositions, most sulfide inclusions in diamond from the No. 50 kimberlite were probably trapped as monosulfide crystals, although some may have been entrapped as melts.

Keywords: electron probe microanalysis and microscopy; solid-phase mineral inclusion; Fuxian kimberlite; metasomatic event; diamond formation



Citation: Zhao, D. Electron Probe Microanalysis and Microscopy of Polishing-Exposed Solid-Phase Mineral Inclusions in Fuxian Kimberlite Diamonds. *Minerals* **2022**, *12*, 844. <https://doi.org/10.3390/min12070844>

Academic Editor: David Phillips

Received: 3 June 2022

Accepted: 27 June 2022

Published: 30 June 2022

Publisher's Note: MDPI stays neutral with regard to jurisdictional claims in published maps and institutional affiliations.



Copyright: © 2022 by the author. Licensee MDPI, Basel, Switzerland. This article is an open access article distributed under the terms and conditions of the Creative Commons Attribution (CC BY) license (<https://creativecommons.org/licenses/by/4.0/>).

1. Introduction

Natural diamond often contains mineral or fluid inclusions that provide information about the chemical and physical environment in the upper mantle. Primary mineral inclusions in diamond can be assigned to either peridotitic (P-type) or eclogitic (E-type) paragenesis [1,2], corresponding to the two major mantle xenolith types; they may also be divided into two categories: primary and secondary. Primary inclusions formed before or during growth of the diamond hosts. They usually do not have fractures connected to the outside of the host and are completely contained in diamond. Primary inclusions have been protected by the diamond host since they were entrapped. On the other hand, secondary inclusions, those that formed after the formation of the diamond hosts or by modification of primary inclusions exposed to the surrounding environment through fractures in the diamond crystal, usually have a fracture connected to the outside of diamond host. Secondary inclusions provide ambiguous records of multi-stage processes, for example, during eruption of the host kimberlitic magma. Knowledge of chemical composition of inclusions allows reconstruction of diamond growth conditions (e.g., P-T-fO₂) and thus

contributes to an understanding of upper mantle processes. Primary inclusions usually occur as crystals, albeit with negative crystal faces, or as amorphous substances. In terms of mineral species, inclusions in diamond include silicate, sulfide, and more rarely carbonate, oxide, carbide, and native elements (graphite, diamond, metals and alloys). A favorable tectonic environment for diamond is present in three cratons in China, the North China or Sino-Korean, the Yangtze, and the Tarim Cratons. In the North China craton, hundreds of kimberlite diatremes and dikes have been located [3]. The kimberlite cluster in Fuxian (now called Wafangdian), Liaoning Province is at the south end of the East Liaoning Uplift of the North China craton and has more than 100 kimberlite bodies. Previous studies on mineral inclusions in diamond from the Fuxian kimberlite mostly focused on specific and unusual types of inclusions [3–21], for example, silicon carbide in diamond by [5], high-Cu and high-Cl inclusions by Chen et al. [13], a carbon-rich multiphase inclusion by Wang et al. [12], syngenetic inclusion geochemistry by Harris et al. [16] and Meyer et al. [17], and native metals and alloys by Gorshkov et al. [20]. Some of these studies are qualitative, without compositional data, and some do not indicate whether the inclusions are primary or secondary. To systematically study mineral inclusions in diamond from the No. 50 kimberlite diatreme in the North China craton, we used the polishing technique to expose mineral inclusions in diamond. A total of 355 diamond crystals with inclusions were examined. Among them, more than 100 diamonds were polished to expose the mineral inclusions for further studies. These diamonds were selected from thousands of diamonds produced by the Liaoning Sixth Geological Exploration Team.

2. Geology of the Fuxian Kimberlite

The Fuxian kimberlites are located about 60 km west of Kaiyuan-Yingkou fault and 30–40 km east of the Tanlu Fault, a major NNE-trending transcurrent structure in East China extending thousands of kilometers from Northeastern to Central China. In the Fuxian area, from north to south, there are three parallel kimberlite zones. The northern zone is medially rich in diamond and consists of numerous kimberlite pipes and dikes, including China's largest kimberlite body, the No. 42 diatreme (4000 m² on the surface). The central zone, also called Toudaogou zone, is most rich in diamond. The famous No. 50 diatreme is situated in the central zone. In the neighboring gullies, some dikes and diamond placers are present. The other kimberlite bodies in the central zone include No. 51, 68 and 74 diatremes and some dikes. The southern zone is poor in diamond and consists of small kimberlite bodies. Country rocks of the Fuxian kimberlite are the Proterozoic Nanfen and Qiaotou Formations. The Nanfen Formation consist mainly of shale with some siltstone and occurs in the southwest part of the kimberlite area. The Qiaotou Formation consists predominantly of thick quartz sandstone with some thin siltstone and occurs in the whole area. The highest stratigraphic level of sediment intruded by the Fuxian kimberlite is the Maozhuang Formation of middle Cambrian age. It was estimated that about 1000–1500 m of metasediments were eroded away at the No. 50 diatreme, while at the No. 42 diatreme, the depth of metasediments eroded could be more than 1500 m [3]. The Fuxian kimberlite is believed to have been emplaced about 400 to 500 Ma ago [3]. Diabase dikes or sills also occur in this area and sometimes cut through the kimberlite bodies (Liaoning Sixth Geological Team 1990, unpublished manuscript).

The No. 50 kimberlite diatreme occurs as an irregular rhombus on the ground. The long axis of the diatreme is in an east–west direction and extends for about 275 m; the short axis is in south–north direction and extends for about 65 m. The diatreme dips 85° to the southeast. The upper and middle parts of the No. 50 diatreme consist mainly of kimberlite tuff breccia. Kimberlite from the No. 50 and No. 42 diatremes has inequigranular texture. Alteration such as serpentinization and carbonatization of the kimberlite is extensive and strong. Primary phenocryst/xenocryst minerals include olivine, phlogopite, pyrope, chromite, diamond, and zircon. The matrix consists primarily of late-stage olivine, phlogopite, carbonate, apatite, magnetite, chromite, anatase, perovskite, rutile, zircon, wollastonite and diopside [3].

3. Sample Preparation

Typically, most of mineral inclusions in the diamond are extracted by crushing or burning diamond hosts. The shortcomings of these two techniques include contamination and oxidation of mineral inclusions and difficulties in recovering small inclusions. Recently, polishing has been employed to reveal mineral inclusions in diamond [22]. The size of the inclusions in diamond exposed by polishing may be as small as 5 μm , whereas inclusions extracted from diamond by mechanical crushing are generally larger than 30 μm in diameter [23,24].

The sample preparation procedure is as follows. An inclusion-bearing diamond is first cleaned in ethanol or alcohol ultrasonically three times (use acetone to clean the crystal bond). The shape, size, and color of a diamond and its inclusions (if any) are examined and described with an optical microscope. A clean specimen mold or bottle cap is used to produce an epoxy resin disk with a diamond crystal. The mold is then labeled with the sample number and some mold release is applied to help remove resin from the mold after its solidification. The cleaned diamond is then oriented on a piece of double-sided sticky tape on the bottom of the mold so that the (111) face of a diamond is not parallel to the bottom of the mold. This orientation will avoid polishing of the hardest (111) face of the diamond. A second way to avoid polishing of the (111) face is to polish the sample at a direction that is not parallel to the bottom of the mold. Liquid resin (epoxy:hardener = 5:1) is gently poured into the mold and vacuumed to get rid of bubbles. After ~24 h, the solidified resin disc with diamond can be removed from the mold. The resin disc is then polished carefully by using diamond-impregnated polishing wheels (diamond size 70, 30 or 15 μm). A 15- μm diamond wheel is effective enough for final polishing for chemical characterization using electron probe microanalysis (EPMA), also called electron microprobe analysis (EMPA), although a 6- μm diamond wheel is better. A brand new diamond wheel polishes diamond crystal very quickly. The detailed sample preparation procedure was documented by Zhao [25].

4. Analytical Methods

A variety of analytical techniques, including backscattered electron (BSE) imaging from scanning electron microscopy (SEM), qualitative analysis and mapping of X-ray energy dispersive spectroscopy (EDS), quantitative analysis from EPMA wavelength dispersive spectroscopy (WDS), and micro-Raman spectroscopy, were employed to characterize mineral inclusions and diamond hosts. Species of mineral inclusions can be qualitatively identified using EDS because many phases have a characteristic or unique EDS spectrum. Such identification is routinely performed with SEM and EPMA and the results are usually reliable, especially when combined with other methods, such as optical microscopy and EPMA WDS quantitative analysis. BSE and EDS data were acquired on the Hitachi S-570 SEM or the Cameca CAMEBAX electron microprobe at the University of Michigan. Mineral inclusions, mostly olivine, to be identified by micro-Raman were not polished to the surface since micro-Raman beam has ability to penetrate into diamond host. The micro-Raman spectra were acquired using a Renishaw Raman microscope at the University of Michigan.

Compositions of mineral inclusions were determined quantitatively on the Cameca CAMEBAX electron microprobe equipped with four spectrometers. Element concentrations were determined by WDS with a PAP correction routine. Most mineral inclusions were analyzed with a focused beam in a spot mode, but carbonates and water-bearing phases were analyzed with a raster mode. Peak and background counting times were set at 30 and 15 s, except for Si in chromite, which was counted for 120 s to increase precision. Background positions were adjusted when two backgrounds were significantly different. To examine homogeneity, multiple points were acquired for each phase.

Natural and synthetic materials were used as standards. For analysis of silicate minerals (such as olivine, pyroxene, and garnet), an accelerating voltage of 15 kV and a beam current of 10 nA were used. The standards used are clinopyroxene (from Irving) as a standard for Si and Ca, olivine for Mg, ferrosilite for Fe, almandine (from Ingamells) for Al,

uvarovite for Cr, geikielite for Ti, rhodonite for Mn, NiS for Ni, and jadeite (from ANU) for Na. For analysis of spinel/chromite analyses, ferrosilite (synthetic) was used as standard for Si, geikielite (synthetic) for Mg and Ti, chromite for Al, V₂O₅ (synthetic) for V, Cr₂O₃ (synthetic) for Cr, rhodonite (Broken Hill) for Mn, hematite (Elba) for Fe, and NiS (synthetic) for Ni. Spinel was analyzed at an accelerating voltage of 10 kV and a beam current of 45 nA. The lower voltage was used to reduce the potential secondary fluorescence effect of Cr by Fe [26]. Chromite inclusions in diamond may contain higher Si content than other chromites. To increase the precision and accuracy of Si measurements, the counting time for Si in chromite inclusions was intentionally set at 120 s. For sulfide, FeS (synthetic) was used as standard for S and Fe, Scott chalcopyrite for Cu, NiS (synthetic) for Ni, ZnS (synthetic) for Zn, MnS (synthetic) for Mn and CoS (synthetic) for Co. Sulfide was analyzed at an accelerating voltage of 20 kV and a beam current of 10 nA or at 10 kV and 20 nA if K and Cr were included. The lower voltage was also used to reduce the fluorescence effect of Fe by Ni.

5. Features of Diamond Hosts and Their Mineral Inclusions

The diamond crystals were optically examined for color, size, crystal form, fractures, and mineral inclusions. Most of the diamonds from the No. 50 kimberlite diatreme are colorless and transparent; some diamond crystals are light yellow, light brownish yellow, light gray, milky white or brown; occasionally, diamond crystals are light blue, light yellowish green, pink or black [3]. The size of the diamond ranges from 1 to 3 mm in diameter. The diamond is mainly single crystal. The common forms are step-like octahedron, curved-face rhombic dodecahedron, perfect octahedron, and combined forms; twinned diamond (for example, macles) or aggregated crystals were also identified but are rare. The partial resorption of octahedra along edges can be observed. Some single crystals are distorted while others possess perfect crystal forms. Simple and combined crystal forms of diamonds were recognized under the binocular microscope and by using a goniometer. The common crystal forms include the following: octahedra, o{111}, usually layered; dodecahedra, d{110}, curved or layered faces. Other shapes, such as cube, hexoctahedron, tetrahedron, etc. are rare [15].

About 40% of the diamond crystals contain graphite, and approximately 0.8% diamond crystals have silicates and other inclusions [3]. A preliminary visual inspection under a binocular microscope showed that the most common mineral in the diamond is graphite in the form of gray or black flakes. Inclusion phases were visually examined for associated fractures to the diamond surface. Most mineral inclusions in diamond were first exposed on the polished surface of diamond using the polishing procedure described above. After optical examination, mineral inclusions were characterized by SEM, micro-Raman, and EPMA, if the inclusions were large enough. Table 1 shows the inclusions identified in the diamonds of the No. 50 kimberlite. Except for graphite, these mineral inclusions are almost exclusively peridotitic, with olivine being the most abundant inclusion, followed by chromite, pyrope, sulfide, orthopyroxene, Ca-carbonate, magnesite, and a Fe-dominant phase (Figure 1). There are often two or more, same or different inclusions in one diamond crystal. Inclusion shapes are generally octahedral, often flattened or elongated (e.g., Figure 1a), showing that the negative crystals of the inclusion morphology had been imposed by the diamond host [27].

Olivine inclusions are very common (Figure 1b,c and Figure 2). Multiple olivine inclusions can occur in the same diamond or associated with other minerals. For example, in the diamond LN50D04, there are two olivine inclusions and one chromite inclusion (Figure 2c). Sometimes two olivine inclusions have different orientations in a diamond. For example, in the diamond LN50D03 (Figure 2b), the c axis of the larger olivine is perpendicular to the polished section, while the c axis of the smaller one is close to parallel to the polished section. The olivine inclusions are euhedral (Figure 2b,d), elongated (Figure 2g,i), subhedral (Figure 2h), or anhedral (Figure 2f). The form of an olivine inclusion is often strongly constrained by the crystal form of the diamond host. The bent feature

of the olivine crystal in the diamond LN50D45 (Figure 2g) might be evidence of such constraint. The ring structure surrounding the olivine in the diamond LN50D04 (Figure 2d) may be the result of strain between the inclusion and the diamond host.

Table 1. Mineral inclusions identified in diamonds from the No. 50 kimberlite diatreme.

Protogenetic/Syngenetic		Epigenetic	Uncertain
Ultramafic	Eclogitic		
forsterite *	Omphacite [3,20]	calcite *	phlogopite [3,20]
enstatite *	coesite (quartz) [9]	magnesite *	magnetite [20]
Diopside [3,15,20]	rutile [20]	graphite *	apatite [3,20]
pyrope *	ilmenite [20]		moissanite [5]
spinel *	graphite *		graphite *
ilmenite [20]			native iron [9,20]
sulfides *			Fe-dominant phase *
zircon [20]			Cr-Fe-Ni alloy [20]
diamond *			
graphite *			
native iron [9,20]?			
native chromium [20]?			
magnesite *			
Ca-carbonate *			
hydrous Mg-silicate *			

* This work.

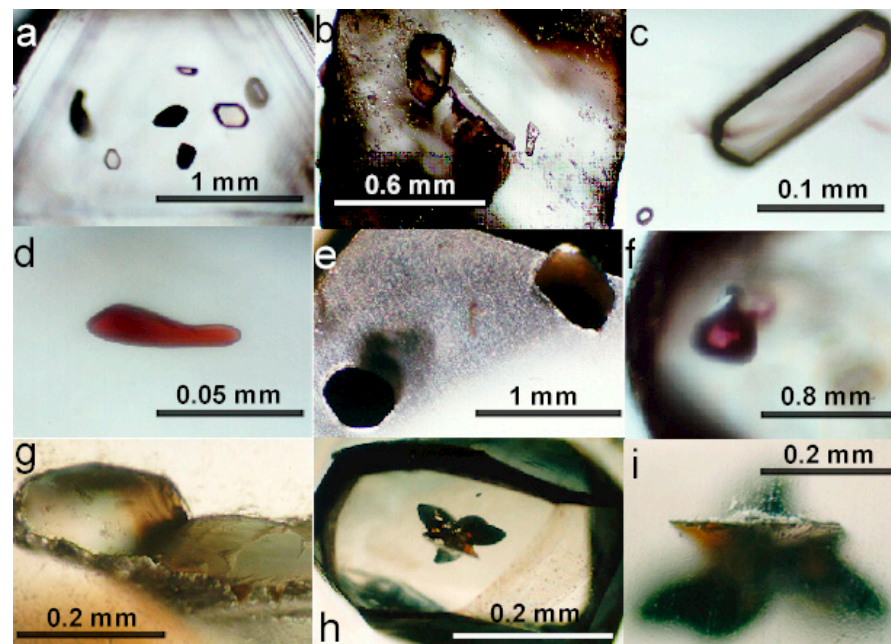


Figure 1. Transmitted plane-polarized light images of diamond hosts and their mineral inclusions. (a) Multiple inclusions in the diamond LN50D12 with at least 7 inclusions (4 olivine and 3 chromite). (b) Inclusions of two larger and one smaller olivine in the diamond LN50D02. There are some black platelets over the surface of the small euhedral elongated olivine inclusion. (c) Two olivine inclusions distributed along a NE direction in the diamond LN50D04. (d) An irregular chromite inclusion in the diamond LN50D04. (e) Two chromite inclusions in the diamond LN50D07. The upper right chromite inclusion is only partly included in the diamond host. (f) Garnet (purple, on the left) and olivine (lower right corner) inclusions in the diamond LN50D10. (g) Two orthopyroxene inclusions in the diamond LN50D40. (h) Butterfly-like graphite inclusion in the diamond LN50D38. (i) Enlarged image of the graphite inclusion in (h). X-ray mapping of the fracture shows no Si, indicating that the inclusions are not SiC.

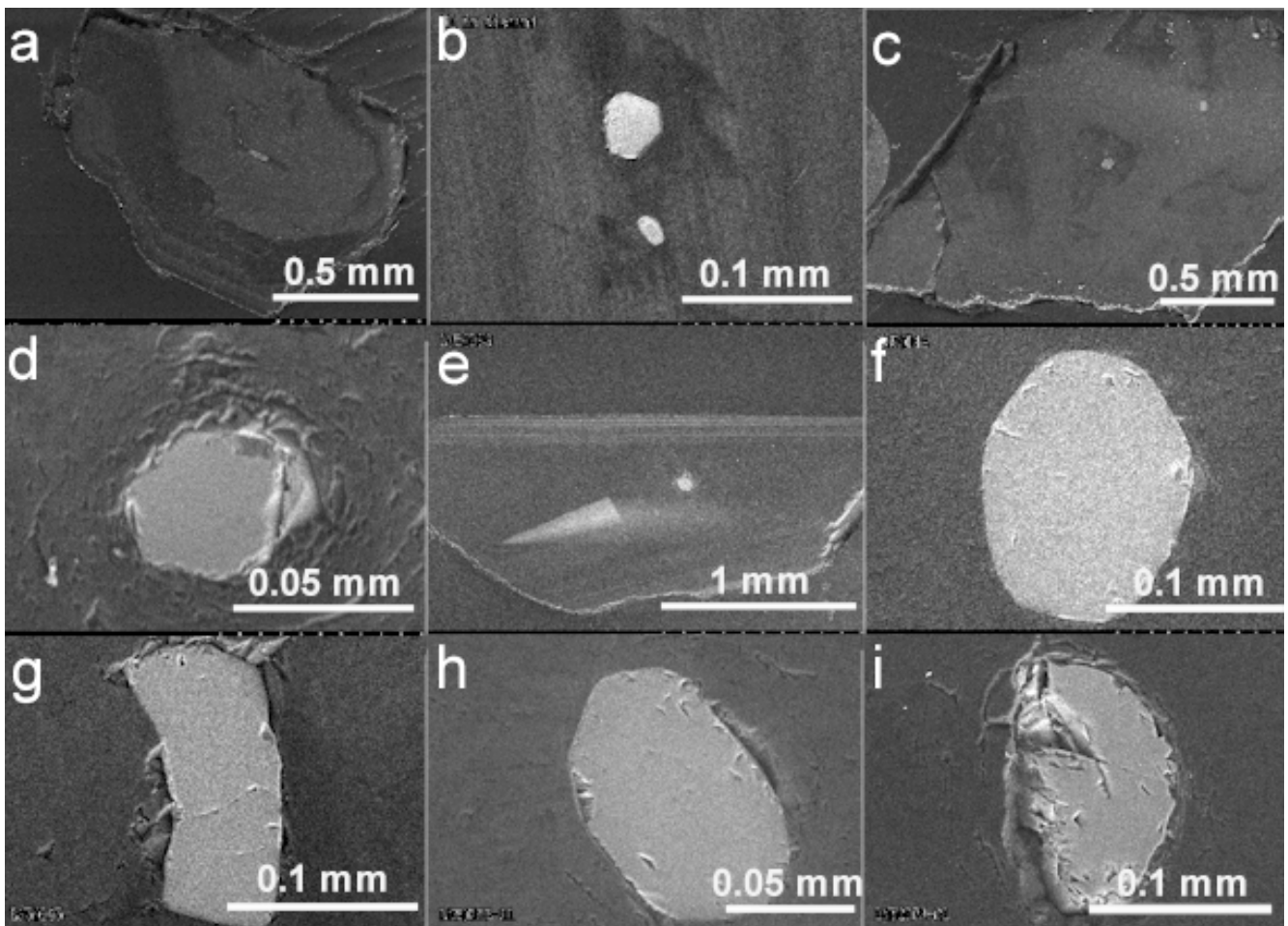


Figure 2. Backscattered electron images of diamond hosts and their olivine mineral inclusions (reproduced from [21] with permission from Cambridge University Press). (a) Diamond LN50D03 and an elongated olivine inclusion. Note the cathodoluminescent pattern of the diamond host. (b) A second polished surface of the diamond LN50D03 with two euhedral olivine inclusions. The c axis of the large olivine is perpendicular to the polished section, while the c axis of the small olivine is close to parallel to the polished section. (c) Two olivine inclusions and one chromite inclusion at the upper right corner in the diamond LN50D04. Note the cathodoluminescent pattern surrounding the olivine at the center. (d) The euhedral olivine inclusion at the center of the diamond LN50D04. Note the ring structure surrounding the olivine inclusion, a possible result of strain between the inclusion and the host. (e) Diamond LN50D39 with an olivine inclusion and a triangular cathodoluminescent pattern. (f) One anhedral olivine inclusion in the diamond LN50D44. (g) One euhedral olivine inclusion in the diamond LN50D45. Note the bent feature of the inclusion that was possibly constrained by the crystal form of diamond host or simply trapped as such during the formation of the diamond. (h) One subhedral olivine inclusion in the diamond LN50D55. (i) One elongated olivine inclusion in the diamond LN50D68.

Chromite inclusions are also common (Figure 1d,e and Figure 3). Like olivine, there are often two or more chromite inclusions in a diamond (LN50D07, Figure 3a). The crystals of chromite inclusions are subhedral (LN50D12, Figure 3d) or euhedral (LN50D58, Figure 3f). Interestingly, small chromite inclusions tend to form perfect crystal forms, which may indicate that the chromite crystals form negative crystal faces imposed by the diamond host, and are located close to the center of the host (Figure 3e), while larger chromites are usually anhedral or subhedral and are distributed near the edge of the diamond (Figure 3a). In the diamond LN50D07, there are three chromite inclusions, of which two touch each other and the third one is separate (Figure 3a). The smallest chromite occurs

in the outermost zone of cathodoluminescence, but all the three chromites are close to the edge of the diamond, indicating that the inclusions were trapped at the later stages of diamond growth. The euhedral chromite at the center of cathodoluminescent pattern of the diamond LN50D58 (Figure 3e) indicates that the inclusion was trapped at the early stage of diamond growth.

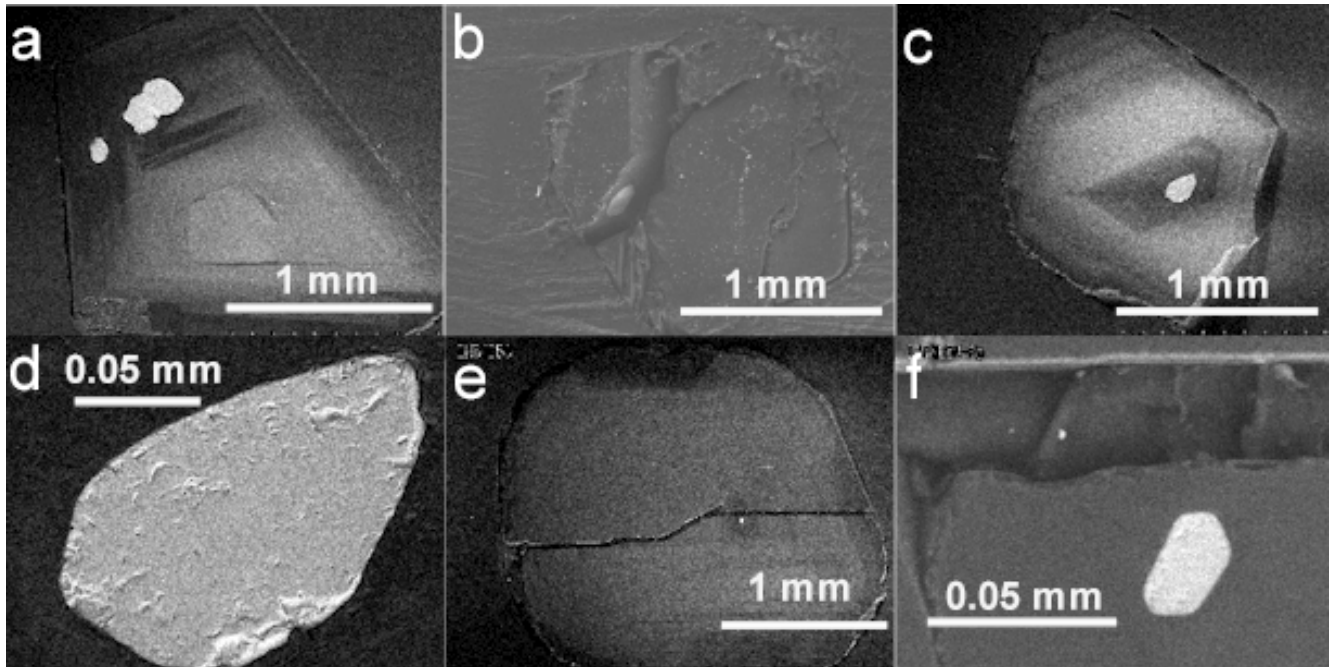


Figure 3. BSE images of diamond hosts and their chromite mineral inclusions. (a) Diamond LN50D07 and three chromite inclusions distributed along the edge of cathodoluminescent pattern. (b) Diamond LN50D45 and a chromite inclusion in the broken fracture developed during polishing. (c) Diamond LN50D12 and a chromite inclusion at the center of cathodoluminescent pattern. (d) The chromite inclusion in (c) at higher magnification. (e) Diamond LN50D58 and a tiny (30 μm) chromite inclusion. The diamond host was broken during polishing. (f) The euhedral chromite inclusion in (e) at higher magnification.

Garnet was identified in a few diamond crystals (Figures 1f and 4). The diamond LN50D10 has two garnet inclusions, one of which is subhedral (Figure 4b). A garnet inclusion in the diamond LN50D13 (Figure 4c) was broken, and there are fractures connected to the outside, but its composition is similar to those of other garnet inclusions, indicating that it did not form or re-equilibrate after the formation of the diamond host.

Four orthopyroxene inclusions were identified. There are two touching orthopyroxene crystals in the diamond LN50D40 and each is approximately 200 μm (Figures 1g and 5a,b). One green orthopyroxene that is 350 μm long was found in the diamond LN50D65.

Two primary Ca carbonate inclusions were identified in the LN50D11 and LN50D97, respectively, by SEM. One of them was approximately 80 μm in size and was destroyed during further polishing for EPMA (diamond LN50D11, Figure 6a,b). An irregular magnesite inclusion was identified in the diamond LN50D29. Secondary Ca carbonate and magnesite were identified within a fracture in the diamond LN50D13 (Figure 4d).

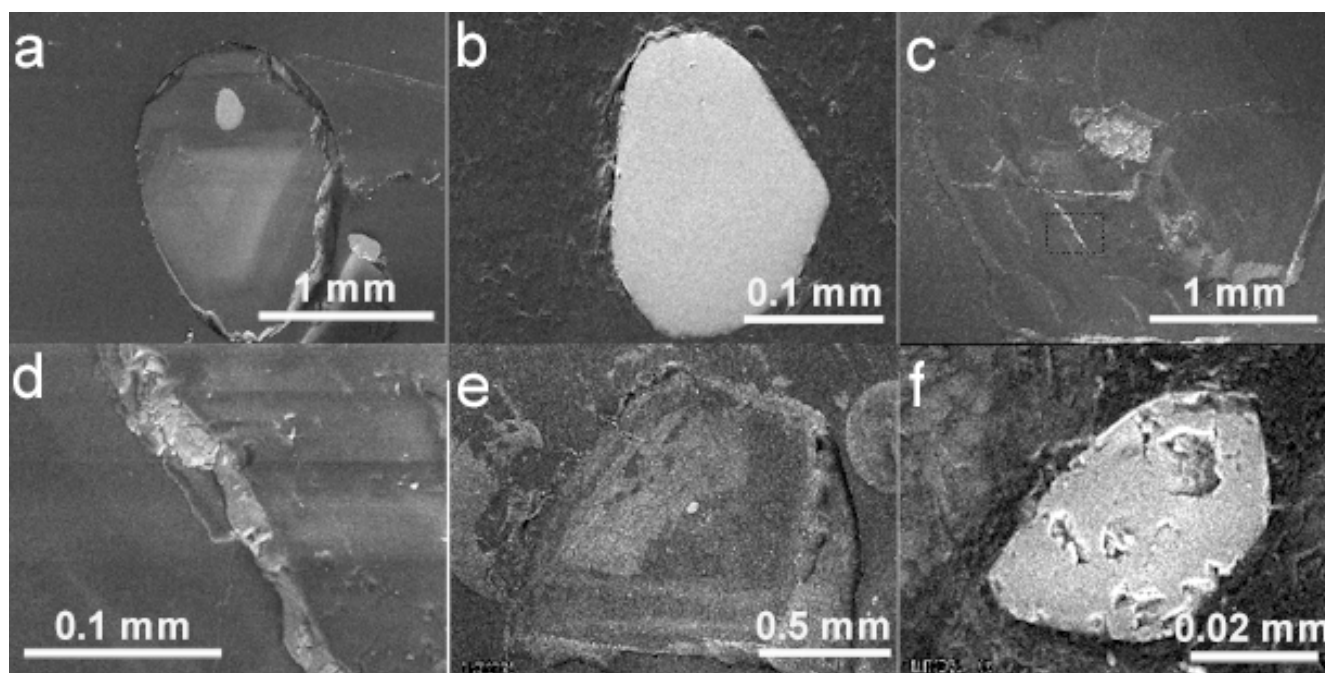


Figure 4. BSE images of diamond hosts and their garnet mineral inclusions. (a) Diamond LN50D10 and a garnet inclusion. (b) The garnet inclusion in (a) at higher magnification. (c) Diamond LN50D13 and a garnet inclusion with fractures connected to the outside. Composition of the relatively large inclusion suggests that it was not formed after the formation of diamond host. (d) Carbonate inclusions in a fracture in the diamond LN50D13 at higher magnification. (e) Diamond LN50D71 and a garnet inclusion. Note the complex cathodoluminescent pattern. (f) The garnet inclusion in (e) at higher magnification.

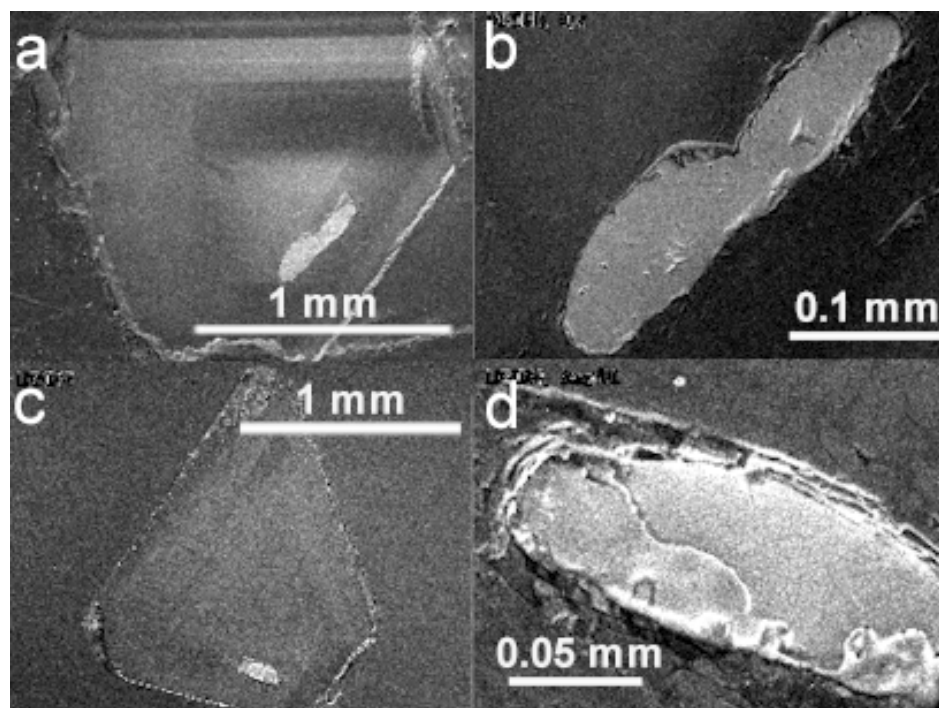


Figure 5. BSE images of diamond hosts and pyroxene and other silicate mineral inclusions. (a) Diamond LN50D40 and two coexisting orthopyroxene inclusions, also showing cathodoluminescent pattern. (b) The orthopyroxene inclusions in (a) at higher magnification. (c) Diamond LN50D67 and an unknown silicate inclusion. (d) The unknown silicate inclusion in (c) at higher magnification.

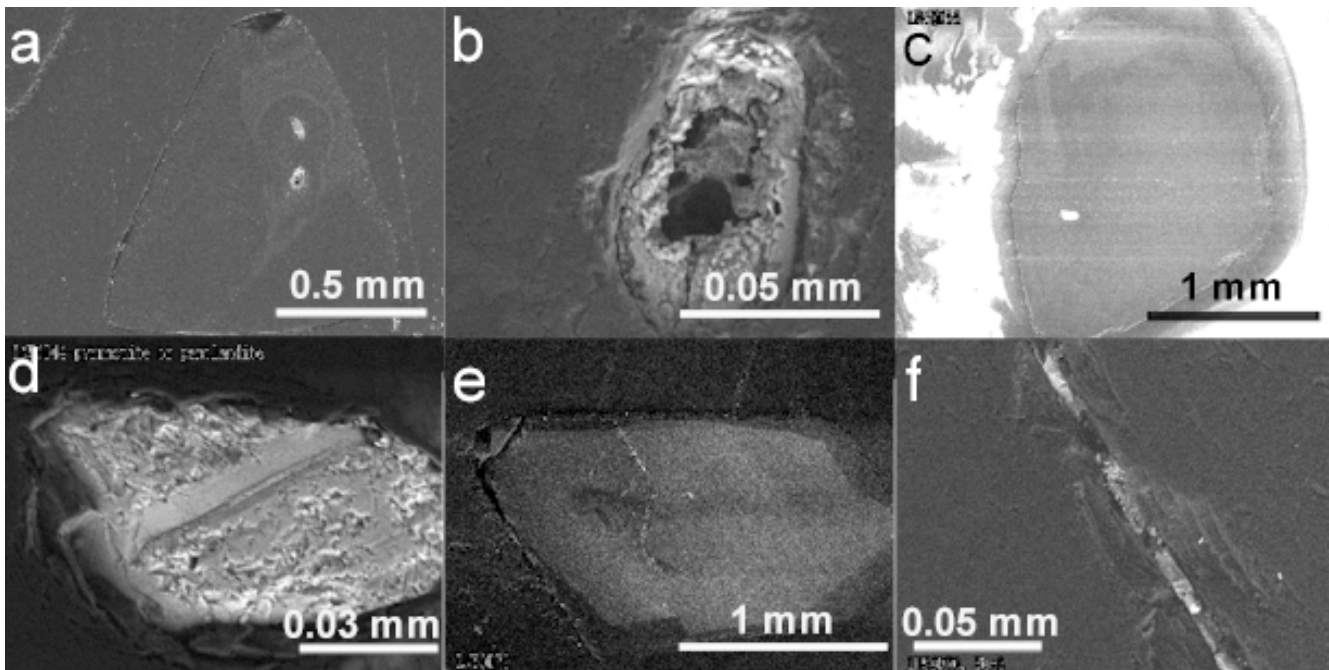


Figure 6. BSE images of diamond hosts and carbonate and sulfide mineral inclusions. (a) Diamond LN50D11 with one Ca-carbonate and one olivine inclusion. (b) The Ca-carbonate inclusion in (a), partly destroyed, at higher magnification. (c) Diamond LN50D42 and a sulfide inclusion. (d) The sulfide inclusion in (c) at higher magnification. (e) Diamond LN50D70 and a protogenetic or syngenetic olivine inclusion close to the center. A fracture extended to the surface of diamond cuts through the cathodoluminescent pattern, indicating that it was developed after the formation of the diamond host. In the top part of the fracture, an epigenetic pyrite inclusion was identified. (f) The epigenetic sulfide inclusion in (e) at higher magnification.

Sulfide inclusions were recovered in diamond samples LN50D04, LN50D32, LN50D37, LN50D42, and LN50D70 (Figure 6c,f). Most sulfide inclusions in diamond are primary (Figure 6c,d) and range from 20 to 50 μm in size. Primary sulfide inclusions are usually associated with internal fractures in diamond, and the fractures are filled with graphite. One secondary sulfide inclusion was found in a fracture that extended to the diamond surface (Figure 6e,f). This secondary sulfide inclusion is about 15 μm long, smaller than most primary sulfide inclusions.

Graphite inclusions are the most abundant, and occur as flakes or as aggregates of flakes, like a butterfly, in internal fractures or fractures extended to the outside (Figure 1h). On the crystal faces of some olivine inclusions, there are tiny (1–2 μm) black platelets (Figure 1b). Black dendritic materials are also found in the interfaces of diamond and inclusion. According to Harris [28], these black platelets on the surface of mineral inclusions are graphite. A special effort was made to find moissanite (SiC), an inclusion reported in the No. 50 diatreme diamond [5], but none was found. X-ray mapping of the fracture filled with graphite and sulfide in the diamond LN50D32 shows no Si counts, indicating that there is not any SiC inclusion in this fracture.

Other inclusions extracted by polishing include an unknown (hydrous) magnesium silicate (LN50D67, Figure 5c,d), an Fe-rich phase (LN50D09), and diamond (LN50D35 and LN50D36). A diamond is included in another diamond, indicating that diamond is of multistage genesis. Diopside, omphacite, phlogopite, rutile, zircon, magnetite [20], ilmenite, apatite [3,20], coesite [9], silicon carbide [5], native iron [9,20], native chromium and Cr-Fe-Ni alloy [20] have also been reported as inclusions in the Fuxian diamonds, but they were not encountered in this work (Table 1).

6. Results and Discussion

6.1. BSE Images and Cathodoluminescence of Diamond Hosts

The BSE images of polished sections of diamond often show certain cathodoluminescent patterns (e.g., Figure 2a,c,e). The internal structures of diamond revealed by cathodoluminescence include the following: (1) zoned patterns, e.g., sample LN50D3 (Figure 2a) has two distinctive bright and dark zones on the BSE image; (2) triangular patterns, e.g., in samples LN50D39 (Figure 2e) and LN50D40 (Figure 5a). The cathodoluminescent patterns surrounding the inclusions at the centers of diamonds LN50D04 (Figure 2c), LN50D12 (Figure 3c) and LN50D58 (Figure 3e) suggest that some inclusions may have served as the seed of diamond growth. The internal structure of diamond revealed by cathodoluminescence and the relative position of inclusions in the diamond host allow the variation of the chemistry of the inclusion over time during the growth of the host diamond to be investigated. Mineral inclusions in the same cathodoluminescent zone of a diamond may have formed at the same time and under the same P-T conditions. Therefore, meaningful P-T conditions calculated from mineral inclusion assemblages in the diamond host must come from the same cathodoluminescent zone.

6.2. EDS and X-ray Mapping of Mineral Inclusions

EDS qualitative identification of mineral inclusions could be affected by sample preparation and its geometric relation with the EDS detector. A phase to be identified must be on the surface and there must be no substance blocking the characteristic X-rays reaching the detector. If an inclusion is located in an unevenly broken fracture or is blocked by the diamond host, characteristic X-rays from an inclusion may not be able to reach the detector, due to the geometry between detector and sample. For example, the diamond host LN50D45 was broken during polishing and an inclusion was exposed on the downward fracture surface (Figure 3b). To avoid loss of the inclusion, the sample was subsequently imaged and identified with SEM and EDS without further polishing. Initially, only Cr and C peaks were identified in the EDS spectra of the inclusion, seemingly suggesting that the inclusion phase is native Cr or CrC. However, when the same sample was coated with carbon and put into the SEM chamber again with 180° rotation horizontally, elements O, Mg, Al, Cr and Fe were detected in the EDS in the upper part of the inclusion, indicating the inclusion is chromite. However, in the lower part of the inclusion, still only Cr and C peaks were detected. X-ray mapping of elements in the chromite inclusion also did not detect light elements in the lower part of the inclusion. Clearly an EDS spectrum can be strongly affected by sample geometry and position of the detector relative to the sample. The reported native Cr in carbonado and diamond by [20,29] contains Cr peak and tiny O and Al peaks, suggesting that chromite might have been misidentified as Cr metal.

X-ray mapping is often used to determine homogeneity or heterogeneity of a phase or intergrowth. In Figure 7, X-ray maps of sulfide inclusions in diamond show a heterogeneous distributions in S, Fe, Ni and Cu, consistent with the EPMA results.

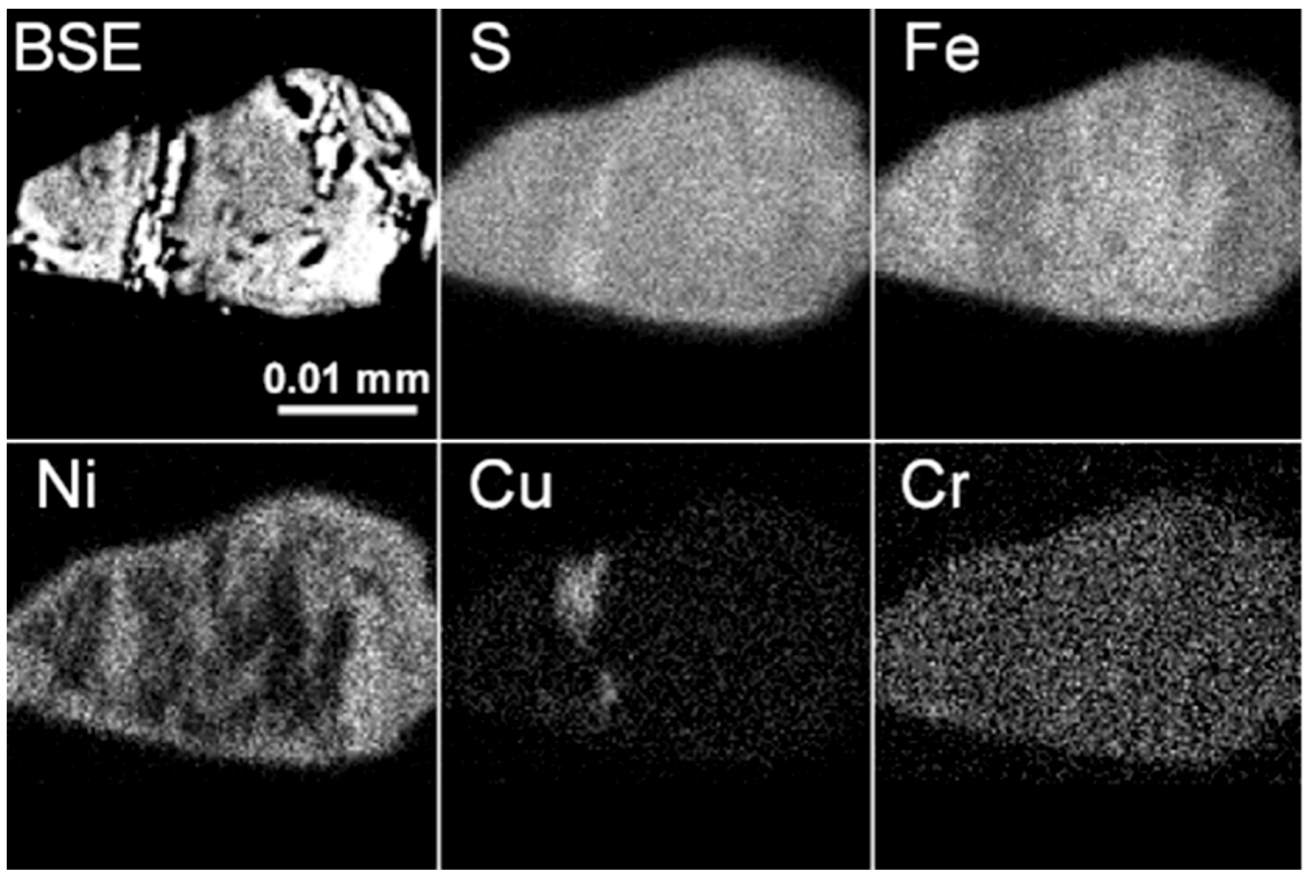


Figure 7. X-ray mapping of elements in a sulfide inclusion in the diamond LN50D04. Fe, Ni, Cu and S are heterogeneously distributed and Cu is much enriched in some areas.

6.3. Micro-Raman Spectra of Mineral Inclusions

Micro-Raman spectroscopy was used to identify mineral species of inclusion phases in diamond qualitatively. The micro-Raman technique provides structural information of phase and allows distinction of different polymorphs of the same composition, for example, olivine, wadsleyite and ringwoodite with $(\text{Mg,Fe})_2\text{SiO}_4$. It also has the capability to penetrate into the diamond host. Therefore, an inclusion that is still completely included in diamond but close to the polished surface may be identified by its micro-Raman spectrum. Three micro-Raman spectra were obtained for three olivine inclusions (Figure 8): one olivine inclusion is on the polished surface of the diamond (LN50D68); a second olivine inclusion is below the polished surface (LN50D73); a third olivine is also below the polished surface (LN50D96). These inclusions (Figure 8) have clearly visible peaks around 820 and 850 cm^{-1} , consistent with the main olivine Raman peaks [30], (indicating that the $(\text{Mg,Fe})_2\text{SiO}_4$ phases identified by EPMA (see below) are not wadsleyite or ringwoodite. Wadsleyite and ringwoodite have main peaks at 721 and 918 cm^{-1} , and 796 and 841 cm^{-1} , in the range of 500 to 1300 cm^{-1} , respectively [31]. In addition, the olivine inclusion exposed on the surface (Figure 8a) has stronger peaks around 820 and 850 cm^{-1} than those below the polished surface (Figure 8b,c). Some low EPMA totals of olivine inclusions are probably caused by the lower surface of inclusion relative to the diamond host due to polishing.

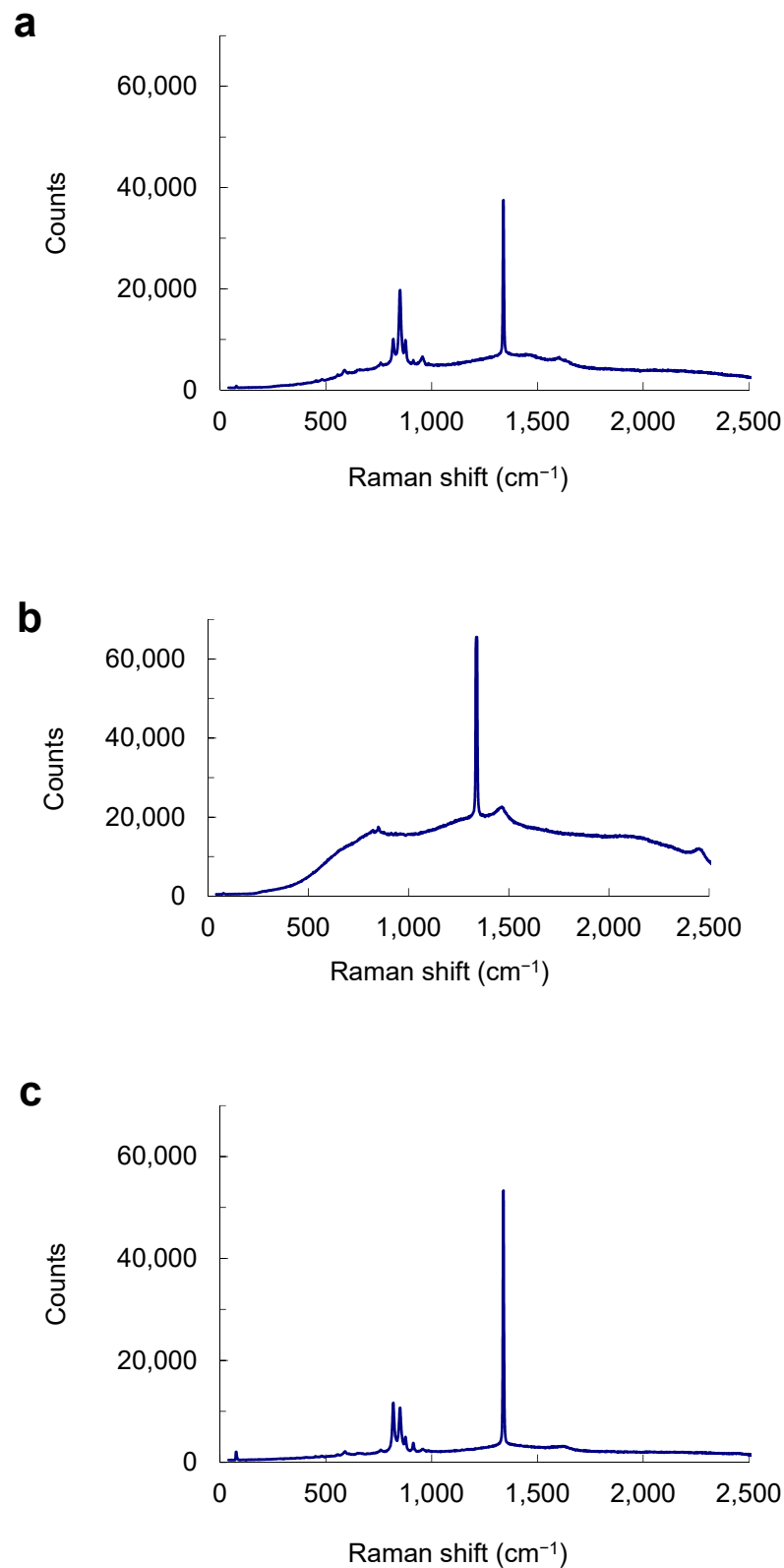


Figure 8. Polarized, single-crystal Raman spectra of olivine inclusions. (a) On the polished surface of the diamond LN50D68. (b) Below the polished surface (LN50D73). (c) Below the polished surface with a low EPMA total (LN50D96). Olivine inclusions with normal and low EPMA totals show the same or similar micro-Raman spectra.

6.4. Chemical Compositions of Peridotitic Mineral Inclusions

Chemical compositions of mineral inclusions are presented in Tables 2–8. All mineral inclusions are homogeneous except for sulfide ones.

Olivine. Approximately 47 olivine inclusions were analyzed in this work (Table 2) and additional EPMA analyses of olivine inclusions from the Fuxian kimberlites are also available in the literature [3,16,17]. Olivine inclusions typically have a high Mg # of 92–94. Mg # is defined as $100\text{Mg}/(\text{Mg} + \text{Fe}^{2+})$ by atom where all Fe is assumed to be Fe^{2+} for olivine and Fe^{3+} is calculated in the case of chromite. The peak position for the Mg # of olivine is 93, a value that is slightly lower than average Mg # of 94 for worldwide olivine inclusions [1,32,33], but similar to those of olivine inclusions from the Akwatia diamonds [24]. Only two olivine inclusions have a Mg # that is outside the range of 92–94 (Figure 9a). The NiO contents of the olivine inclusions are usually in the range of 0.25 to 0.45 wt. % and are concentrated around 0.4 wt. % (Table 2; Figure 9b). One exceptional value is for the olivine from the diamond LN50D62, which has up to 0.80 wt. % NiO. Due to the wide NiO range (0.25–0.45 wt. %), the constant Ni content assumption for mantle olivine for the Ni-in-garnet thermometer may not always be valid [34,35].

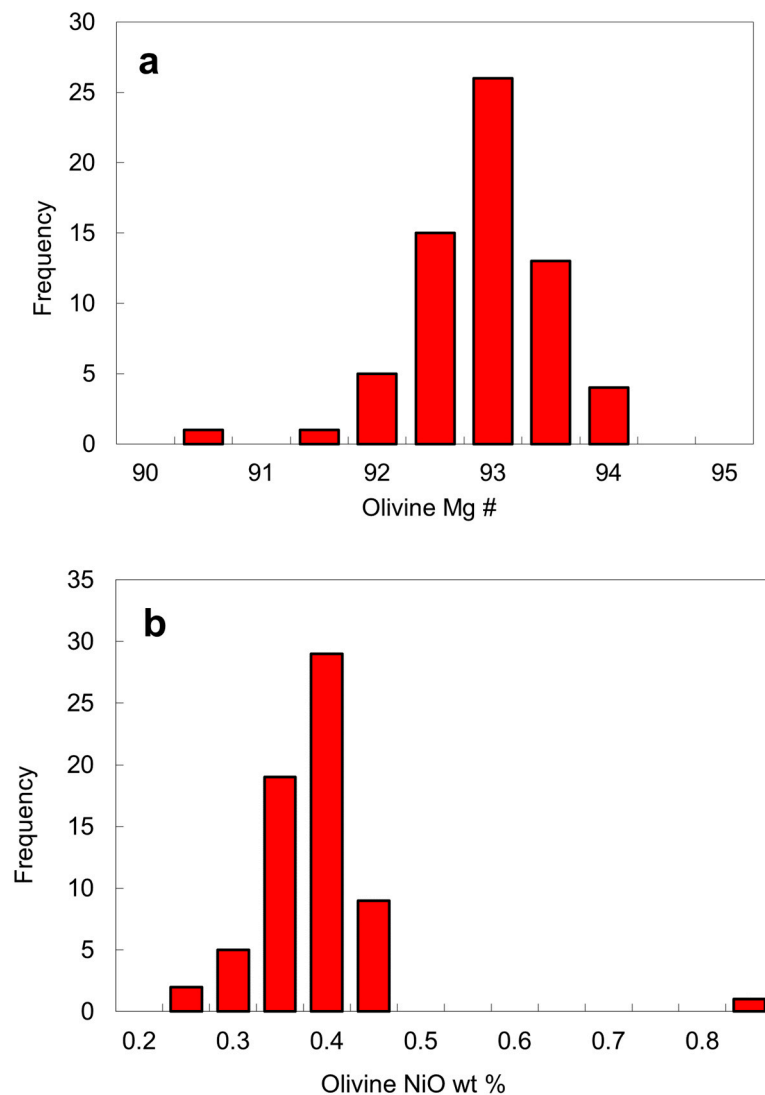


Figure 9. Histograms of olivine inclusions in diamond from the No. 50 kimberlite diatreme: (a) Mg # defined as $100\text{Mg}/(\text{Mg} + \text{Fe}^{2+})$ by atom, where all Fe in olivine is assumed to Fe^{2+} ; (b) NiO contents. The data are from Table 2.

Table 2. Average compositions of olivine inclusions in diamonds from the No. 50 kimberlite diatreme.

Sample	LN50D01	LN50D02	LN50D02	LN50D03	LN50D03	LN50D03	LN50D04	LN50D04	LN50D06	LN50D06	LN50D06	LN50D11	LN50D11
Inclusion		1 (large)	2 (small)	1 (small)	2 (large)	3	1	2	1	2	3	1	2
SiO ₂	41.21	39.98	40.61	41.08	41.36	41.22	41.38	42.02	41.20	40.69	40.69	40.58	41.14
TiO ₂	0.01	0.00	0.00	0.00	0.00	0.01	0.01	0.00	0.01	0.00	0.01	0.01	0.00
Al ₂ O ₃	0.01	0.01	0.02	0.01	0.01	0.02	0.01	0.01	0.00	0.01	0.02	0.00	0.01
Cr ₂ O ₃	0.05	0.04	0.04	0.08	0.08	0.13	0.07	0.09	0.07	0.06	0.04	0.04	0.02
TFeO	7.39	7.33	7.11	6.38	6.52	6.35	6.48	6.39	7.08	7.24	7.05	7.49	7.56
NiO	0.37	0.35	0.34	0.34	0.35	0.39	0.34	0.26	0.37	0.36	0.34	0.39	0.38
MnO	0.11	0.10	0.10	0.09	0.13	0.06	0.11	0.09	0.09	0.12	0.12	0.11	0.09
MgO	51.28	51.32	51.17	51.62	51.74	51.14	51.27	51.72	51.35	51.02	50.98	50.72	50.18
CaO	0.02	0.03	0.04	0.02	0.03	0.02	0.02	0.03	0.03	0.03	0.04	0.04	0.04
Na ₂ O	na	na	na	na	na	0.02	0.00	0.00	na	na	na	na	0.02
Σ	100.45	99.17	99.42	99.62	100.22	99.37	99.69	100.61	100.20	99.53	99.29	99.37	99.44
Si	0.994	0.975	0.988	0.995	0.997	1.003	1.004	1.009	0.996	0.990	0.992	0.990	1.005
Al	0.000	0.000	0.000	0.000	0.000	0.001	0.000	0.000	0.000	0.000	0.001	0.000	0.000
Ti	0.000	0.000	0.000	0.000	0.000	0.000	0.000	0.000	0.000	0.000	0.000	0.000	0.000
Cr	0.001	0.001	0.001	0.002	0.001	0.002	0.001	0.002	0.001	0.001	0.001	0.001	0.000
Fe	0.149	0.149	0.145	0.129	0.131	0.129	0.132	0.128	0.143	0.147	0.144	0.153	0.154
Ni	0.007	0.007	0.007	0.007	0.007	0.008	0.007	0.005	0.007	0.007	0.007	0.008	0.007
Mn	0.002	0.002	0.002	0.002	0.003	0.001	0.002	0.002	0.002	0.002	0.002	0.002	0.002
Mg	1.845	1.865	1.856	1.865	1.859	1.854	1.854	1.852	1.850	1.851	1.853	1.845	1.828
Ca	0.001	0.001	0.001	0.000	0.001	0.001	0.000	0.001	0.001	0.001	0.001	0.001	0.001
Na	0.000	0.000	0.000	0.000	0.000	0.001	0.000	0.000	0.000	0.000	0.000	0.000	0.001
Σcation	3.000	3.000	3.000	3.000	3.000	3.000	3.000	3.000	3.000	3.000	3.000	3.000	3.000
ΣO	3.995	3.975	3.989	3.996	3.998	4.004	4.005	4.010	3.997	3.991	3.993	3.991	4.005
Mg #	92.5	92.6	92.8	93.5	93.4	93.5	93.4	93.5	92.8	92.6	92.8	92.4	92.2

Table 2. Cont.

LN50D12	LN50D12	LN50D14	LN50D14	LN50D20	LN50D21	LN50D30	LN50D35	LN50D35	LN50D39	LN50D44	LN50D45	LN50D50	LN50D50
1 (large)	2 (small)	1	2				1 (large)	2 (small)				1 (large)	2
41.52	40.92	40.94	40.48	40.81	40.83	39.71	41.13	41.18	41.34	41.54	41.11	40.76	40.95
0.02	0.00	0.00	0.01	0.00	0.01	0.01	0.01	0.00	0.00	0.01	0.00	0.01	0.00
0.05	0.12	0.04	0.34	0.02	0.02	0.02	0.01	0.01	0.02	0.00	0.01	0.01	0.02
0.08	0.07	0.08	0.05	0.02	0.08	0.04	0.04	0.07	0.08	0.10	0.06	0.05	0.07
7.78	7.56	7.70	7.79	7.73	7.05	8.07	6.87	6.77	7.33	7.59	6.97	7.61	7.92
0.36	0.43	0.42	0.44	0.40	0.35	0.42	0.35	0.30	0.38	0.39	0.45	0.41	0.40
0.11	0.13	0.06	0.12	0.11	0.09	0.13	0.09	0.10	0.15	0.10	0.12	0.12	0.05
50.78	49.89	50.68	50.41	50.90	51.20	49.15	51.62	52.10	50.45	50.86	51.73	50.80	50.35
0.02	0.03	0.04	0.09	0.01	0.03	0.05	0.02	0.02	0.04	0.04	0.03	0.03	0.04
0.02	0.01	0.01	0.01	na	0.01	0.02	0.01	0.01	na	na	0.01	0.01	0.02
100.74	99.14	99.97	99.73	100.01	99.67	97.62	100.15	100.55	99.78	100.63	100.48	99.82	99.82
1.002	1.004	0.995	0.986	0.990	0.991	0.990	0.993	0.989	1.006	1.003	0.989	0.991	0.997
0.001	0.003	0.001	0.010	0.000	0.001	0.001	0.000	0.000	0.001	0.000	0.000	0.000	0.000
0.000	0.000	0.000	0.000	0.000	0.000	0.000	0.000	0.000	0.000	0.000	0.000	0.000	0.000
0.002	0.001	0.002	0.001	0.000	0.002	0.001	0.001	0.001	0.001	0.002	0.001	0.001	0.001
0.157	0.155	0.156	0.159	0.157	0.143	0.168	0.139	0.136	0.149	0.153	0.140	0.155	0.161
0.007	0.008	0.008	0.009	0.008	0.007	0.008	0.007	0.006	0.007	0.008	0.009	0.008	0.008
0.002	0.003	0.001	0.002	0.002	0.002	0.003	0.002	0.002	0.003	0.002	0.002	0.002	0.001
1.827	1.825	1.835	1.831	1.842	1.853	1.827	1.858	1.865	1.831	1.831	1.856	1.841	1.828
0.001	0.001	0.001	0.002	0.000	0.001	0.001	0.000	0.000	0.001	0.001	0.001	0.001	0.001
0.001	0.000	0.000	0.000	0.000	0.000	0.001	0.001	0.000	0.000	0.000	0.001	0.000	0.001
3.000	3.000	3.000	3.000	3.000	3.000	3.000	3.000	3.000	3.000	3.000	3.000	3.000	3.000
4.003	4.006	3.996	3.991	3.991	3.993	3.990	3.993	3.990	4.007	4.004	3.990	3.992	3.998
92.1	92.2	92.1	92.0	92.1	92.8	91.6	93.1	93.2	92.5	92.3	93.0	92.3	91.9

Table 2. Cont.

LN50D69	LN50D69	LN50D69	LN50D70	LN50D72	LN50D74	LN50D79	LN50D91	LN50D91	LN50D91	LN50D91	LN50D94	LN50D95	LN50D96	LN50D99
1 (large)	2 (small)						1 (large)	2 (small)	3	4				
40.54	41.21	41.06	41.39	41.83	40.75	40.87	41.70	40.82	40.76	40.98	41.29	41.27	40.19	41.01
0.01	0.00	0.00	0.01	0.00	0.02	0.01	0.01	0.01	0.00	0.00	0.01	0.00	0.01	0.00
0.02	0.03	0.02	0.01	0.05	0.04	0.00	0.01	0.01	0.01	0.01	0.01	0.01	0.02	0.00
0.10	0.07	0.06	0.06	0.08	0.06	0.07	0.03	0.06	0.05	0.03	0.03	0.04	0.03	0.04
6.82	6.65	6.67	6.53	7.29	6.75	6.94	7.68	7.61	7.75	7.65	6.85	6.72	7.29	7.08
0.34	0.36	0.35	0.31	0.36	0.29	0.35	0.36	0.36	0.33	0.34	0.36	0.32	0.33	0.40
0.12	0.07	0.06	0.06	0.14	0.12	0.10	0.11	0.09	0.06	0.08	0.11	0.10	0.07	0.04
50.78	50.33	51.82	50.85	50.94	51.12	50.92	51.39	50.84	51.13	51.27	51.94	51.55	50.73	52.02
0.06	0.03	0.05	0.02	0.03	0.02	0.03	0.03	0.02	0.02	0.02	0.04	0.02	0.04	0.01
0.00	0.02	0.03	0.01	0.01	0.00	0.01	0.01	0.00	0.01	0.01	0.00	0.00	0.01	0.01
98.78	98.76	100.12	99.24	100.74	99.17	99.30	101.32	99.81	100.12	100.38	100.64	100.05	98.72	100.61
0.993	1.011	0.990	1.009	1.008	0.993	0.996	0.999	0.992	0.987	0.990	0.992	0.997	0.985	0.985
0.000	0.001	0.001	0.000	0.002	0.001	0.000	0.000	0.000	0.000	0.000	0.000	0.000	0.001	0.000
0.000	0.000	0.000	0.000	0.000	0.000	0.000	0.000	0.000	0.000	0.000	0.000	0.000	0.000	0.000
0.002	0.001	0.001	0.001	0.002	0.001	0.001	0.001	0.001	0.001	0.001	0.001	0.001	0.001	0.001
0.140	0.136	0.134	0.133	0.147	0.138	0.141	0.154	0.155	0.157	0.154	0.138	0.136	0.149	0.142
0.007	0.007	0.007	0.006	0.007	0.006	0.007	0.007	0.007	0.006	0.007	0.007	0.006	0.007	0.008
0.002	0.001	0.001	0.001	0.003	0.002	0.002	0.002	0.002	0.001	0.002	0.002	0.002	0.002	0.001
1.854	1.841	1.863	1.848	1.830	1.858	1.850	1.836	1.842	1.846	1.846	1.859	1.857	1.854	1.863
0.002	0.001	0.001	0.001	0.001	0.001	0.001	0.001	0.000	0.001	0.001	0.001	0.001	0.001	0.000
0.000	0.001	0.002	0.000	0.001	0.000	0.000	0.001	0.000	0.000	0.000	0.000	0.000	0.000	0.000
3.000	3.000	3.000	3.000	3.000	3.000	3.000	3.000	3.000	3.000	3.000	3.000	3.000	3.000	3.000
3.994	4.011	3.990	4.010	4.009	3.995	3.997	3.999	3.993	3.988	3.990	3.992	3.998	3.986	3.985
93.0	93.1	93.3	93.3	92.6	93.1	92.9	92.3	92.3	92.2	92.3	93.1	93.2	92.5	92.9

Mg # = 100Mg/(Fe + Mg) by atoms; na: not analyzed; Fe³⁺ not calculated.

Table 3. Compositions of chromite inclusions in diamonds from the No. 50 kimberlite diatreme.

Sample Grain	LN50D03	LN50D04				LN50D07				LN50D12	LN50D20		LN50D58	
		Sp2	Sp 3	Sp 4	Sp 5	Sp 1	Sp 2	Sp 3	Sp 4	Sp	Sp 1	Sp 2	Sp 1	Sp 2
SiO ₂	0.20	0.18	0.16	0.19	0.19	0.12	0.12	0.11	0.15	0.17	0.14	0.14	0.16	0.21
TiO ₂	0.20	0.22	0.19	0.18	0.17	0.41	0.32	0.42	0.41	0.45	0.05	0.06	0.03	0.04
Al ₂ O ₃	6.28	5.83	6.08	5.77	5.88	4.83	4.82	4.82	4.73	4.20	4.92	4.96	6.72	4.76
Cr ₂ O ₃	64.80	66.76	66.48	65.93	65.34	66.10	66.31	66.28	66.74	66.72	64.26	65.00	64.31	66.90
V ₂ O ₃	0.18	0.14	0.16	0.17	0.14	0.16	0.17	0.18	0.22	0.30	0.25	0.26	0.14	0.19
TFeO	13.38	13.41	13.25	13.32	13.24	15.41	15.39	15.16	15.03	15.79	16.42	16.62	13.76	14.22
NiO	0.00	0.09	0.15	0.10	0.13	0.04	0.13	0.09	0.14	0.16	0.08	0.09	0.15	0.00
MnO	0.00	0.23	0.00	0.00	0.00	0.00	0.00	0.00	0.00	0.00	0.24	0.32	0.00	0.00
MgO	14.22	13.74	14.23	13.28	14.43	12.74	12.72	13.46	13.43	12.56	11.96	12.08	13.70	13.37
ZnO	0.10	0.04	0.07	0.07	0.01	0.05	0.03	0.09	0.06	0.08	0.09	0.08	0.06	0.03
Σ	99.36	100.64	100.77	99.01	99.55	99.86	100.00	100.60	100.90	100.43	98.41	99.61	99.03	99.71
Fe ₂ O ₃	2.10	1.26	1.71	0.78	2.41	1.84	1.88	2.57	2.27	1.89	2.78	2.84	2.02	1.80
FeO	11.49	12.28	11.71	12.62	11.08	13.76	13.70	12.84	12.99	14.09	13.92	14.07	11.94	12.60
Σ	99.57	100.77	100.94	99.09	99.79	100.05	100.19	100.86	101.13	100.62	98.69	99.90	99.24	99.90
Si	0.006	0.006	0.005	0.006	0.006	0.004	0.004	0.004	0.005	0.006	0.005	0.005	0.005	0.007
Alvi	0.242	0.224	0.232	0.226	0.227	0.189	0.188	0.186	0.182	0.164	0.196	0.195	0.261	0.185
Fe ³⁺	0.052	0.031	0.042	0.019	0.059	0.046	0.047	0.063	0.056	0.047	0.071	0.071	0.050	0.045
Ti	0.005	0.005	0.005	0.005	0.004	0.010	0.008	0.010	0.010	0.011	0.001	0.002	0.001	0.001
Cr	1.678	1.719	1.702	1.729	1.690	1.733	1.737	1.717	1.726	1.747	1.715	1.714	1.673	1.749
V	0.005	0.004	0.004	0.004	0.004	0.004	0.005	0.005	0.006	0.008	0.007	0.007	0.004	0.005
Fe ²⁺	0.315	0.335	0.317	0.350	0.303	0.382	0.380	0.352	0.355	0.390	0.393	0.392	0.329	0.348
Ni	0.000	0.002	0.004	0.003	0.003	0.001	0.003	0.002	0.004	0.004	0.002	0.002	0.004	0.000
Mn	0.000	0.006	0.000	0.000	0.000	0.000	0.000	0.000	0.000	0.000	0.007	0.009	0.000	0.000
Mg	0.694	0.667	0.687	0.657	0.704	0.630	0.628	0.658	0.655	0.620	0.602	0.601	0.672	0.659
Zn	0.002	0.001	0.002	0.002	0.000	0.001	0.001	0.002	0.001	0.002	0.002	0.002	0.001	0.001
Σcation	3.000	3.000	3.000	3.000	3.000	3.000	3.000	3.000	3.000	3.000	3.000	3.000	3.000	3.000
ΣO	4.000	4.000	4.000	4.000	4.000	4.000	4.000	4.000	4.000	4.000	4.000	4.000	4.000	4.000
Mg #	68.8	66.6	68.4	65.2	69.9	62.3	62.3	65.1	64.8	61.4	60.5	60.5	67.2	65.4
Cr #	87.4	88.5	88.0	88.5	88.2	90.2	90.2	90.2	90.4	91.4	89.8	89.8	86.5	90.4

Mg # = 100Mg/(Fe²⁺ + Mg) and Cr # = 100Cr/(Cr + Al) by atom; ferric iron by charge balance and stoichiometry.

Table 4. Compositions of garnet inclusions in diamond from the No. 50 kimberlite diatreme.

Sample	LN50D10	LN50D10	LN50D13	LN50D19	LN50D68	LN50D7140A	43A	52A	WG1	WG5	WG6	WG7	WG8	L1	L2	L3	L4	
SiO ₂	41.83	42.38	41.22	40.78	41.05	40.52	42.83	42.21	41.24	41.49	41.70	41.00	41.34	40.22	41.50	40.60	41.20	42.00
TiO ₂	0.04	0.03	0.07	0.05	0.05	0.09	0.02	0.05	0.41	0.02	0.01	0.02	1.08	0.00	0.01	0.03	0.00	0.00
Al ₂ O ₃	19.19	19.13	15.29	14.64	18.06	15.34	18.56	21.94	22.27	18.84	13.50	13.50	15.26	15.23	14.40	13.60	16.40	17.30
Cr ₂ O ₃	6.66	6.78	11.29	13.59	7.46	13.38	6.74	1.76	1.48	6.61	12.80	12.70	8.42	10.37	12.10	12.70	9.90	8.10
TFeO	5.43	5.46	6.66	6.15	6.69	5.88	6.08	7.66	10.36	6.99	6.52	6.52	7.75	6.23	5.95	5.65	6.19	6.99
NiO	0.03	0.03	0.05	0.00	0.05	0.03	0.00	0.00	0.00	0.00	0.00	0.00	na	na	0.00	0.02	0.01	0.07
MnO	0.22	0.17	0.22	0.15	0.24	0.21	0.36	0.32	0.38	0.39	0.35	0.36	0.15	0.21	0.30	0.32	0.26	0.38
MgO	23.11	22.65	22.04	21.59	20.52	21.64	23.52	21.04	19.77	20.01	21.60	21.00	19.05	20.80	21.70	22.00	23.70	20.30
CaO	2.91	3.01	3.25	3.51	5.83	2.79	2.30	4.85	4.31	5.96	4.23	4.80	6.71	5.68	3.79	3.94	1.67	5.66
Na ₂ O	0.00	0.01	0.01	0.00	0.01	0.03	0.01	0.04	0.07	0.02	0.00	0.00	0.07	na	0.00	0.02	0.01	0.04
Σ	99.42	99.64	100.10	100.46	99.97	99.92	100.42	99.87	100.29	100.33	100.71	99.90	99.83	98.74	99.75	98.88	99.34	100.84
Fe ₂ O ₃	0.65	0.00	1.19	0.55	2.18	0.00	0.15	1.52	2.39	1.28	1.03	1.58	0.42	3.01	0.18	1.97	1.81	0.94
FeO	4.85	5.46	5.59	5.66	4.74	5.88	5.95	6.29	8.21	5.84	5.59	5.10	7.37	3.53	5.79	3.87	4.56	6.15
Σ	99.49	99.64	100.21	100.51	100.18	99.92	100.43	100.02	100.53	100.46	100.81	100.06	99.87	99.04	99.77	99.08	99.52	100.93
Si	2.986	3.026	2.988	2.965	2.960	2.956	3.033	2.993	2.941	2.980	3.027	3.004	3.031	2.956	3.027	2.986	2.972	3.016
Aliv	0.014	0.000	0.012	0.035	0.040	0.044	0.000	0.007	0.059	0.020	0.000	0.000	0.000	0.044	0.000	0.014	0.028	0.000
Alvi	1.601	1.610	1.294	1.219	1.494	1.274	1.549	1.827	1.813	1.575	1.155	1.166	1.318	1.275	1.238	1.165	1.366	1.464
Fe ³⁺	0.035	0.000	0.065	0.030	0.118	0.000	0.008	0.081	0.128	0.069	0.056	0.087	0.023	0.166	0.010	0.109	0.098	0.051
Ti	0.002	0.002	0.004	0.003	0.003	0.005	0.001	0.003	0.022	0.001	0.001	0.001	0.060	0.000	0.001	0.002	0.000	0.000
Cr	0.376	0.383	0.647	0.781	0.425	0.772	0.377	0.099	0.083	0.375	0.735	0.736	0.488	0.603	0.698	0.739	0.565	0.460
Fe ²⁺	0.290	0.326	0.339	0.344	0.286	0.358	0.352	0.373	0.490	0.351	0.340	0.312	0.452	0.217	0.353	0.238	0.275	0.369
Ni	0.002	0.002	0.003	0.000	0.003	0.002	0.000	0.000	0.000	0.000	0.000	0.000	0.000	0.000	0.000	0.001	0.001	0.004
Mn	0.013	0.010	0.013	0.009	0.014	0.013	0.022	0.019	0.023	0.024	0.022	0.022	0.009	0.013	0.019	0.020	0.016	0.023
Mg	2.459	2.410	2.382	2.340	2.205	2.353	2.483	2.224	2.102	2.143	2.337	2.294	2.082	2.279	2.359	2.412	2.549	2.173
Ca	0.223	0.230	0.252	0.273	0.450	0.218	0.174	0.368	0.329	0.459	0.329	0.377	0.527	0.447	0.296	0.311	0.129	0.435
Na	0.001	0.001	0.001	0.000	0.002	0.005	0.001	0.005	0.010	0.003	0.000	0.000	0.010	0.000	0.000	0.003	0.001	0.006
Σcation	8.000	8.000	8.000	8.000	8.000	8.000	8.000	8.000	8.000	8.000	8.000	8.000	8.000	8.000	8.000	8.000	8.000	8.000
ΣO	12.000	12.024	12.000	12.000	12.000	12.003	12.000	12.000	12.000	12.000	12.000	12.000	12.000	12.000	12.000	12.000	12.000	12.000
Mg #	88.3	88.1	85.5	86.2	84.5	86.8	87.3	83.0	77.3	83.6	85.5	85.2	81.4	85.6	86.7	87.4	87.2	83.8
Ca #	8.3	8.7	9.6	10.5	17.0	8.5	6.6	14.2	13.5	17.6	12.3	14.1	20.2	16.4	11.2	11.4	4.8	16.7
Cr #	18.9	19.2	33.1	38.4	21.7	36.9	19.6	5.1	4.3	19.1	38.9	38.7	27.0	31.4	36.0	38.5	28.8	23.9

Ca # = 100Ca/(Ca + Mg) by atom; na: not analyzed; Fe³⁺ by charge balance and stoichiometry. Data from this study unless otherwise indicated. 40A, 43A and 52A: Harris et al. [16]. 40A and 43A also reported by Wang and Guo [18]. WG1, WG5–WG8: Wang and Guo [18]. L1–L4: Meyer et al. [17].

Table 5. Compositions of pyroxene inclusions in diamond.

Orthopyroxene							Clinopyroxene			
Sample	LN50D40	LN50D40	LN50D52	LN50D65	38A	52B	Sample	28B	43B	52B
Grain	1	2					Grain			
SiO ₂	58.24	57.75	57.69	57.39	58.62	56.63	SiO ₂	55.25	55.41	54.48
TiO ₂	0.00	0.02	0.01	0.02	0.00	0.11	TiO ₂	0.07	0.01	0.19
Al ₂ O ₃	0.43	0.62	0.95	0.56	0.51	0.76	Al ₂ O ₃	0.76	1.23	2.35
Cr ₂ O ₃	0.53	0.53	0.49	0.48	0.51	0.13	Cr ₂ O ₃	1.51	0.36	0.64
TFeO	4.30	4.33	4.26	4.59	4.18	7.47	TFeO	1.98	2.52	3.95
NiO	0.16	0.10	0.13	0.10	0.11	0.00	NiO	0.00	0.00	0.00
MnO	0.15	0.12	0.14	0.11	0.14	0.13	MnO	0.09	0.07	0.14
MgO	35.22	35.08	36.41	35.49	35.62	32.22	MgO	18.40	18.23	16.97
CaO	0.42	0.42	0.33	0.74	0.26	2.29	CaO	20.89	21.48	18.75
Na ₂ O	0.11	0.12	0.03	0.14	0.00	0.31	Na ₂ O	0.84	0.77	1.81
Σ	99.57	99.09	100.44	99.63	99.95	100.05	Σ	99.79	100.08	99.28
Si	1.002	0.998	0.981	0.986	1.005	0.984	Si	0.999	0.998	0.989
Aliv	0.000	0.002	0.019	0.011	0.000	0.016	Aliv	0.001	0.002	0.011
Alvi	0.009	0.011	0.000	0.000	0.010	0.000	Alvi	0.016	0.024	0.039
Ti	0.000	0.000	0.000	0.000	0.000	0.001	Ti	0.001	0.000	0.003
Cr	0.007	0.007	0.007	0.007	0.007	0.002	Cr	0.022	0.005	0.009
Fe	0.062	0.063	0.061	0.066	0.060	0.108	Fe	0.030	0.038	0.060
Ni	0.002	0.001	0.002	0.001	0.002	0.000	Ni	0.000	0.000	0.000
Mn	0.002	0.002	0.002	0.002	0.002	0.002	Mn	0.001	0.001	0.002
Mg	0.904	0.904	0.923	0.909	0.910	0.834	Mg	0.496	0.490	0.459
Ca	0.008	0.008	0.006	0.014	0.005	0.043	Ca	0.405	0.415	0.365
Na	0.004	0.004	0.001	0.005	0.000	0.010	Na	0.029	0.027	0.064
Σcation	2.000	2.000	2.000	2.000	2.000	2.000	Σcation	2.000	2.000	2.000
ΣO	3.009	3.006	2.993	2.993	3.013	2.988	ΣO	3.005	3.001	2.989
Mg #	93.6	93.5	93.8	93.2	93.8	88.5	Mg#	94.3	92.8	88.5
							Ca#	44.9	45.9	44.3

Mg# = 100Mg/(Fe + Mg) by atoms; Ca# = 100Ca/(Ca + Mg) by atoms; Fe³⁺ not calculated. 38A, 52B, 28B and 43B from Harris et al. [16] and Wang and Guo [18]. 38A: two co-existing opx with the same composition. 52B: websteritic, co-existing clinopyroxene, orthopyroxene and garnet. 28B contains K₂O 0.22 wt % and co-exists with olivine. 43B contains K₂O 0.07 wt % and co-exists with garnet.

Table 6. Representative compositions of sulfide inclusions in diamonds from the No. 50 kimberlite diatreme.

Sample	LN50D04		LN50D32			LN50D37		LN50D42	LN50D70		
Mineral	grg	grg	trl	Cu po	pnt	R ₃ S ₄	R ₃ S ₄	po	py		
Fe	34.13	55.66	31.10	29.81	36.55	37.35	34.43	36.55	36.49	29.54	43.21
Ni	16.73	2.84	33.08	9.78	26.19	13.91	17.33	19.22	18.13	33.75	0.80
Cu	8.64	0.06	0.06	22.00	0.15	0.00	4.65	0.00	0.76	0.33	0.00
Zn	0.00	0.00	0.00	0.00	0.00	0.00	0.00	0.00	0.01	0.00	0.00
Mn	0.00	0.01	0.00	0.00	0.00	0.00	0.00	0.02	0.00	0.01	0.01
Co	0.31	0.00	0.42	0.01	0.30	0.78	0.52	0.67	0.81	0.34	0.80
Cr	na	na	na	na	0.74	0.27	0.37	0.13	0.65	na	na
S	40.47	41.90	36.18	36.54	34.36	49.08	43.18	42.22	43.22	36.23	57.17
Σ	100.29	100.46	100.83	98.15	98.29	101.39	100.47	98.81	100.07	100.18	102.00
	Sulfur normalized to 4										
Fe	1.936	3.051	1.974	1.873	2.442	1.747	1.831	1.988	1.938	1.872	1.736
Ni	0.903	0.148	1.998	0.585	1.665	0.619	0.877	0.995	0.916	2.035	0.030
Cu	0.431	0.003	0.003	1.215	0.009	0.000	0.217	0.000	0.035	0.018	0.000
Zn	0.000	0.000	0.000	0.000	0.000	0.000	0.000	0.000	0.000	0.000	0.000
Mn	0.000	0.000	0.000	0.000	0.000	0.000	0.000	0.001	0.000	0.000	0.000
Co	0.017	0.000	0.025	0.001	0.019	0.035	0.026	0.034	0.041	0.020	0.030
Cr	0.000	0.000	0.000	0.000	0.053	0.013	0.021	0.008	0.037	0.000	0.000
S	4.000	4.000	4.000	4.000	4.000	4.000	4.000	4.000	4.000	4.000	4.000
Σcation	3.287	3.202	4.000	3.674	4.189	2.415	2.972	3.025	2.969	3.947	1.797

grg: greigite; trl: troilite; po: pyrrhotite; pnt: pentlandite; vlr: violarite; py: pyrite. na: not analyzed.

Chromium contents of the olivine inclusions (Table 2; Figure 10a) all fall within the normal reported range of olivine inclusions in diamonds [24] and appear to increase with Mg #, likely owing to different degree of depletion in the mantle. If an olivine inclusion touches or is close to a chromite inclusion in diamond, an apparent high Cr_2O_3 content of the olivine may be caused by secondary X-ray fluorescence of Cr in chromite by Fe in olivine [25,26]. Therefore, a low accelerating voltage (10 kV) is preferred for analysis of olivine inclusions in olivine-chromite pairs in diamond. The unusually high Cr content of olivine inclusions in the Akwatia diamond [24] should be checked for fluorescence effect. Nonetheless, high Cr contents in isolated olivine inclusions are likely be real. Chromium enrichment in olivine might result from specific P-T conditions, crystal-chemical factors, or reduction of Cr, which may enter olivine as Cr^{2+} under reduced conditions [36] or high crystallization temperatures [37,38]. Sutton et al. [39] showed that Cr is predominantly divalent in lunar olivine.

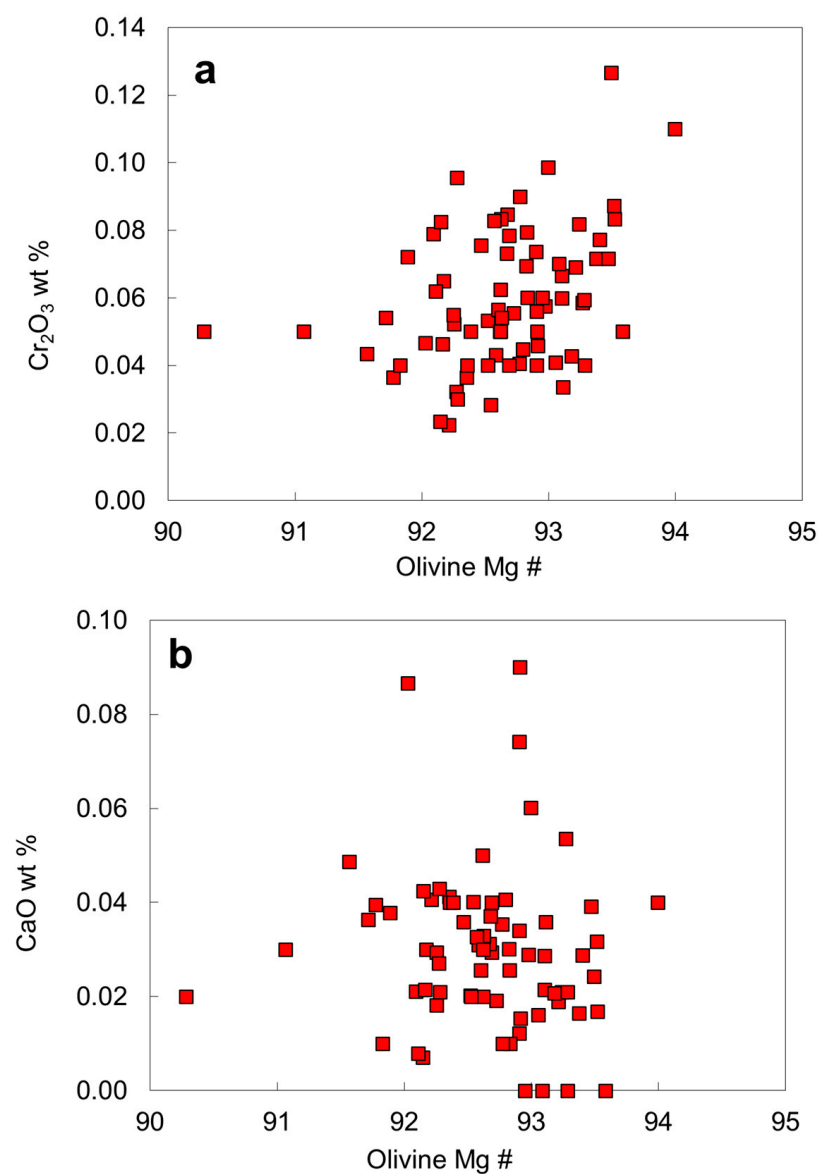


Figure 10. Compositional plots for the olivine inclusions in diamond: (a) Mg # versus Cr_2O_3 ; (b) Mg # versus CaO.

Chromium contents of the olivine inclusions (Table 2; Figure 10a) all fall within the normal reported range of olivine inclusions in diamonds [24] and appear to increase with Mg #, probably due to different degree of depletion in the mantle. If an olivine inclusion touches or is close to a chromite inclusion in diamond, an apparent high Cr₂O₃ content of the olivine may be caused by secondary X-ray fluorescence of Cr in chromite by Fe in olivine [26]. Therefore, a low accelerating voltage (10 kV) is preferred for analysis of olivine inclusions in olivine-chromite pairs in diamond. The unusually high Cr content of olivine inclusions in the Akwatia diamond [24] should be checked for fluorescence effect. Nonetheless, high Cr contents in isolated olivine inclusions are likely to be real. Chromium enrichment in olivine might result from specific P-T conditions, crystal-chemical factors, or reduction in Cr, which may enter olivine as Cr²⁺ under reduced conditions [36] or high crystallization temperatures [37,38]. Sutton et al. [39] showed that Cr is predominantly divalent in lunar olivine.

The Ca content of olivine is an indicator of pressure if it is in equilibrium with clinopyroxene. This is the basis of Ca exchange barometer between olivine and clinopyroxene [40], although it is a system that depends much more on temperature than on pressure [41]. The advantage of applying this system to olivine in diamond is that it is less likely to be reset during late stage processes. Very few olivine inclusions from North China contain CaO exceeding 0.06 wt. % (Table 2; Figure 10b), whereas olivine inclusions in diamond from other localities have CaO mainly in the range 0.00–0.13 and ≤0.23 wt. % [24]. As indicated by the experimental data on Ca exchange between olivine and clinopyroxene [40], a low Ca content in olivine (<0.08 wt. %) would require a high pressure, consistent with diamond stability field. The low Ca content of olivine inclusions might imply a Ca depletion of their source region (i.e., a harzburgite source) or crystallization at a lower temperature or a higher pressure than usual (if from lherzolite).

Chromite. Thirteen chromite inclusions were analyzed (Table 3) and additional chromite analyses from the Fuxian pipes are available in the literature [16–18]. Chromite occurs either as separate inclusions or with other minerals in a single diamond. Diamond commonly contains both chromite and olivine inclusions. The Mg # of the chromite inclusions varies from 60 to 70 with the peak position at a Mg # of 66 (Figure 11), overlapping those of the Fe-rich part of the peridotitic worldwide range (Mg # of 60–80 [24]). Recalculated 100Fe²⁺/(Fe³⁺ + Fe²⁺) ratios are relatively high (76–95), probably indicating a relatively reduced environment. The Al₂O₃ ranges from 4.0 to 7.9 wt. %, within the worldwide range of chromite inclusions in diamond [24]. A striking feature of the chromite inclusions in diamond is a high Cr content (63–67 wt. % Cr₂O₃ Table 3), which lie within the field defined by worldwide chromite inclusions in diamond [1], but are centered around 66 wt. % Cr₂O₃ (Figure 11).

Except for two inclusions with 0.79 and 0.75 wt. % TiO₂, the TiO₂ contents (0.03–0.45 wt. %) of most chromites falls within the compositional range defined by worldwide chromites (maximum 0.65 wt. %), located in the "diamond inclusion field" for chromites (Figure 12a). On a Fe₂O₃ vs. Al₂O₃ diagram, analyses of chromite inclusions fall within a limited compositional range (Figure 12b). The recalculated Fe₂O₃ of the chromite inclusions is less than 4.5 wt. %. The SiO₂ contents of chromite inclusions are high, from 0.08 to 0.29 wt. %, with a pronounced peak around 0.18 wt. % (Figure 11c). The solution of silicate-spinel component is favored by high pressure [42], consistent with the high Cr₂O₃ contents that stabilize spinel towards higher pressures in lherzolites [43].

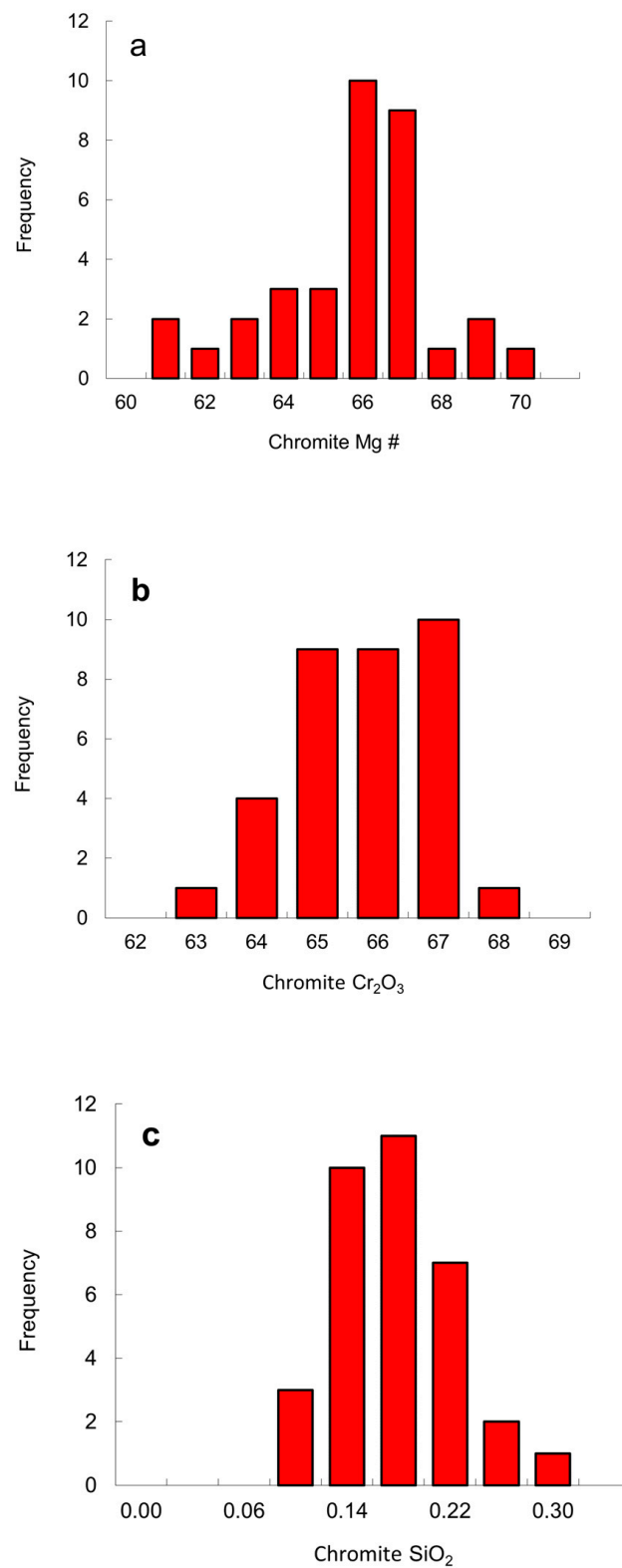


Figure 11. Histograms of chromite inclusions in diamond: (a) Mg #; (b) Cr₂O₃; (c) SiO₂. The data are listed in Table 3.

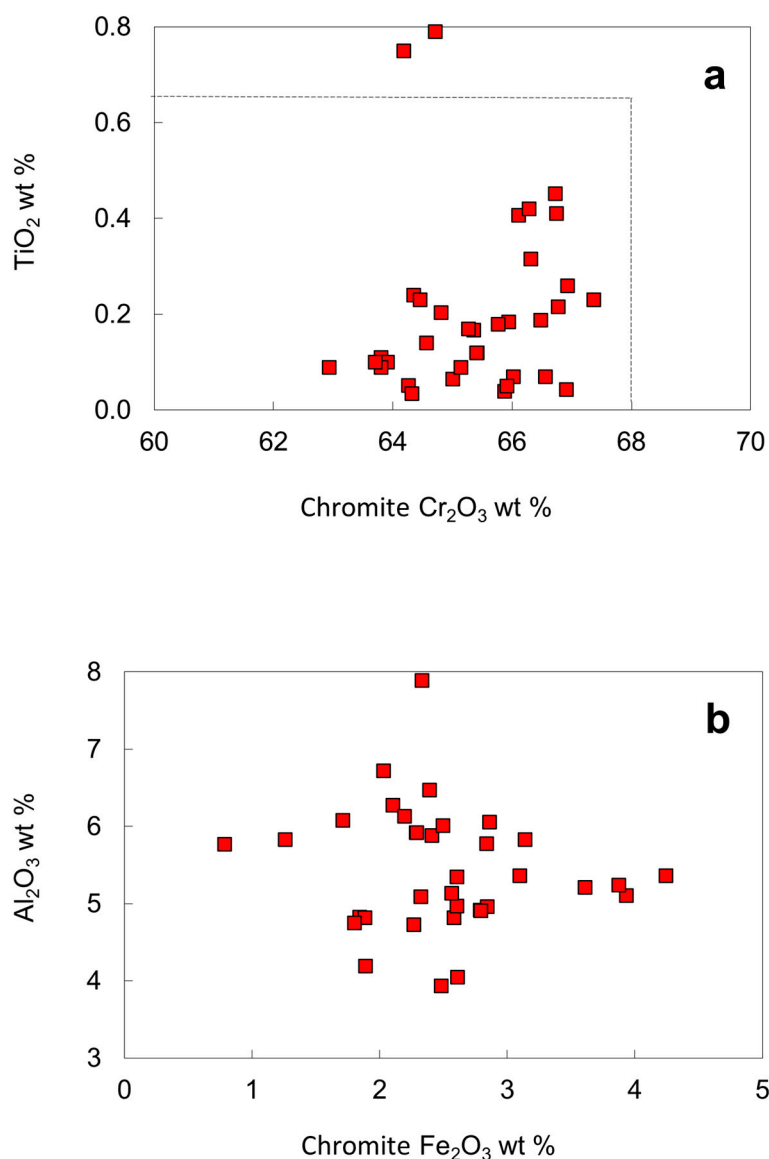


Figure 12. Compositional plots for chromite inclusions in diamond from the No. 50 kimberlite: (a) Cr₂O₃ versus TiO₂; (b) Fe₂O₃ versus Al₂O₃. Dashed lines delineate a "diamond inclusion field" [23]. The total Fe from EPMA is calculated into Fe²⁺ and Fe³⁺.

Some diamonds contain more than one separated chromite inclusion (e.g., samples LN50D04, LN50D07 and LN50D20). Sample LN50D04 has 6 chromite inclusions, some at the edge of the diamond polished section, and others near the center of the diamond host; some are large and euhedral, while others are small and anhedral. There are no significant variations in composition for the multiple spinel grains in the diamond, although such inter-grain compositional variations have been recorded previously [22,23,44,45]. Multiple chromites in a single diamond have nearly the same compositions, probably indicating that the diamond formed in a very short time, or that all the chromite inclusions formed in the same environment, or that the composition of chromite did not evolve during growth of the diamond.

Garnet. Five garnet inclusions in diamond were exposed by polishing and analyzed (Table 4). Garnet occurs either as a single inclusion or together with other mineral phases. Eclogitic garnet is extremely rare. No undisputed eclogitic inclusion was discovered in this study. A garnet numbered 52A in a garnet-orthopyroxene-clinopyroxene assemblage reported by Harris et al. [16] is closest to eclogitic almandine-pyrope. Garnets in diamond

from the No. 50 diatreme have the following: a Mg # of 81–88 (except for sample 52A that coexists with a low magnesian orthopyroxene and clinopyroxene); a Cr # of 19–39 except for samples 43A and 52A, where Cr # is defined as $100\text{Cr}/(\text{Cr} + \text{Al})$ by atom; a Ca # of 5–21, where the Ca # is defined as $100\text{Ca}/(\text{Ca} + \text{Mg})$ by atom (Figure 13).

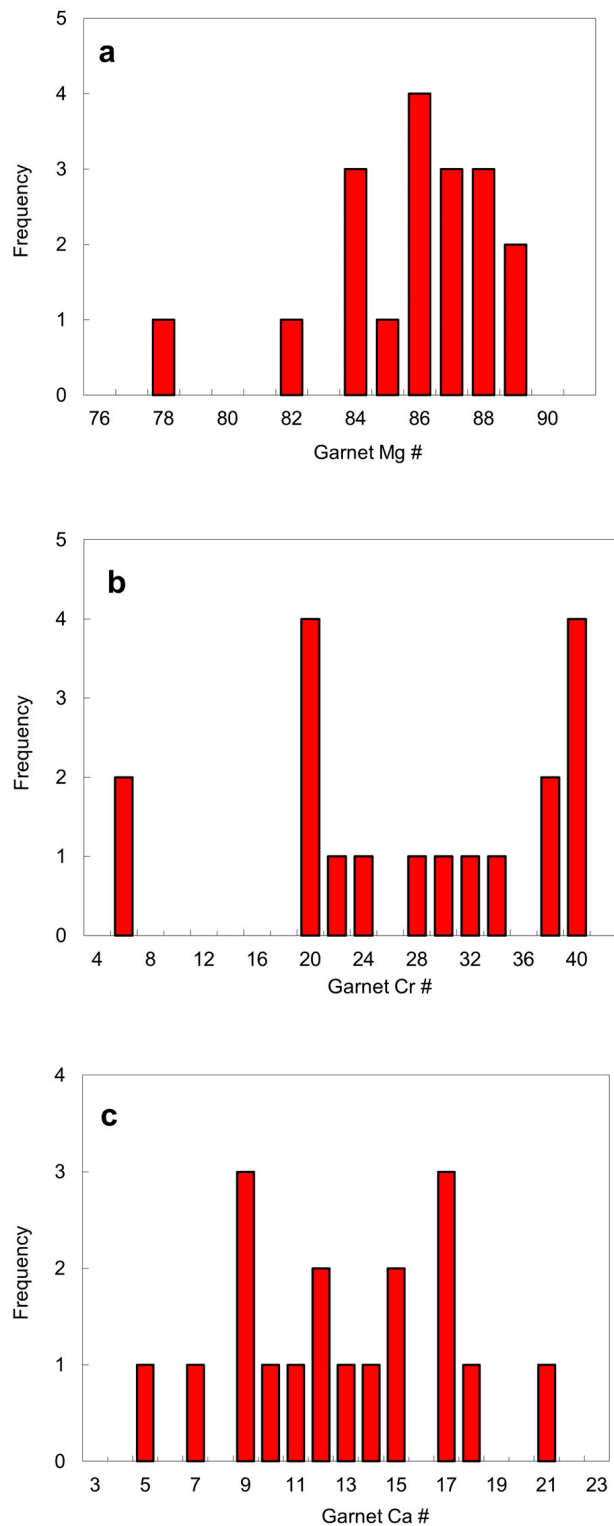


Figure 13. Histograms of garnet inclusions in diamond: (a) Mg #; (b) Cr # defined as $100\text{Cr}/(\text{Cr} + \text{Al})$ by atom; (c) Ca # = $100\text{Ca}/(\text{Ca} + \text{Mg})$ by atom. The data are from Table 4.

To distinguish diamondiferous from non-diamondiferous assemblages on the basis of the composition of peridotitic pyrope, curves on a CaO versus Cr₂O₃ diagram (Figure 14) were derived by various authors [27,46,47] to separate a high (lherzolitic) and a low (harzburgitic) calcium field. Most garnets in diamond from the No. 50 diatreme belong to the harzburgitic paragenesis, and only a few garnet-bearing diamond crystals are part of the lherzolitic association. Chemical compositions of two garnets (samples 43A and 52A, cf. [16]) plot below the dashed line distinguishing peridotitic from non-peridotitic garnets [47], indicating that they may belong to a different paragenesis. The garnet 52A has the lowest Mg # and it also coexists with low Mg # orthopyroxene and clinopyroxene, and therefore the assemblage garnet-orthopyroxene-clinopyroxene may belong to a websterite or eclogitic paragenesis.

Figure 14c shows that only lherzolitic garnets with the lowest Mg # contain significant amounts of TiO₂ (0.41 and 1.08 wt. %), while the other garnets contain less than 0.09 wt. % TiO₂. The Al/Cr ratio in garnet was taken as a measure for the fertility of the source, as there is a positive correlation between Al/Cr ratio and Ti in lherzolitic garnets [24]. However, there is no positive correlation between Al/Cr ratio and Ti content for the garnet inclusions from the No. 50 diamond association.

Most garnet inclusions have Si atoms per formula unit (apfu) close to the ideal value of 3 when normalized to 12 oxygens. A few garnets have Si slightly greater than 3, up to 3.03 apfu (Table 4). The slight excess of Si in garnet may suggest the presence of majoritic component (Mg₃(MgSi)Si₃O₁₂) [32] and further suggests a high-pressure condition if equilibrated with orthopyroxene [48–50]. The diamond LN50D10 has two garnet inclusions. One is small (about 80 µm across) and has no excess Si. The other, exposed after polishing away the first garnet, has a small amount of excess Si (approximately 1%). These two garnets have almost identical compositions except for Si. The difference in Si might be caused by systematic errors between different EPMA sessions. Since one garnet was no longer available, it was not possible to examine systematic errors between different EPMA sessions by analyzing both garnets during a same EPMA session. Therefore, the garnet inclusion with excess Si was re-analyzed, together with a garnet xenocryst sample without excess Si (a Four Corner ultramafic garnet, PY15 [51]). The average of the second garnet inclusion from the second EPMA session has less excess Si (3.003 apfu) relative to the first EPMA session. However, the average of garnet xenocrysts from the same EPMA session also has less Si (2.977 apfu) relative to early EPMA analyses (2.994 apfu). Although inconclusive, these measurements suggest that the small excess Si is real, probably indicating the existence of a very minor majoritic component.

Pyroxene. Four orthopyroxene inclusions in three diamond hosts were recovered (Table 5). In addition, Harris et al. [16] reported two coexisting orthopyroxene inclusions and one websteritic orthopyroxene inclusion. Clinopyroxene was not identified in this work, although six clinopyroxene inclusions were recovered by Harris et al. [16]. Two coexisting orthopyroxene grains in the diamond LN50D40 are homogeneous and have the same composition (Table 5). The Mg # of the orthopyroxene is about 94, except for the websteritic orthopyroxene with a Mg # of 88 (sample 52B, cf. [16]).

The orthopyroxene inclusions have low Ca contents (CaO < 0.50 wt. % except for the websteritic and the green orthopyroxene in LN50D65), probably indicating that some orthopyroxene might not be in equilibrium with clinopyroxene and might represent a harzburgitic origin [52]. Compared to harzburgitic orthopyroxene, the websteritic orthopyroxene has higher Ti, Al, Fe, Ca and Na and lower Si, Cr and Mg (Table 5; Figure 15).

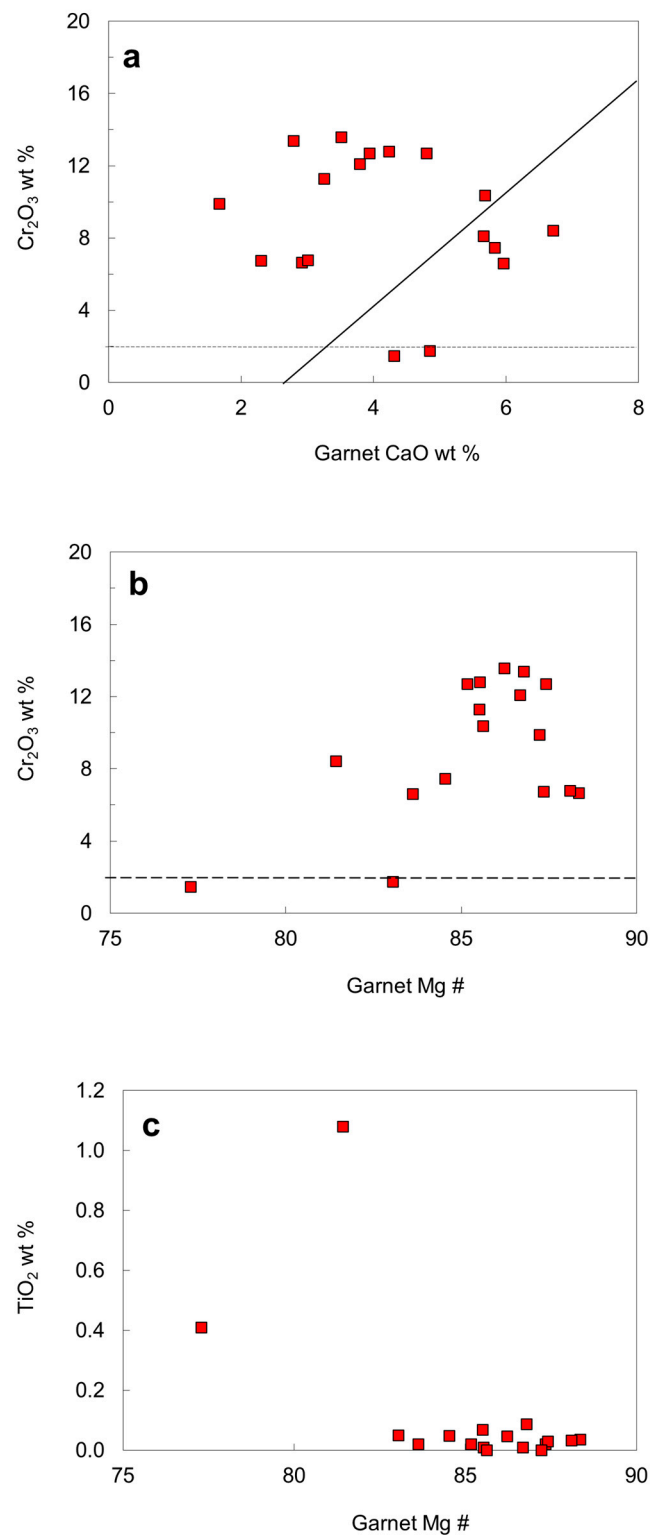


Figure 14. Compositional plots for garnet inclusions in diamond: (a) CaO versus Cr_2O_3 ; (b) Mg # versus Cr_2O_3 ; (c) Mg # versus TiO_2 . Solid line divides compositional fields for lherzolitic and harzburgitic garnets, dashed line distinguishes peridotitic from non-peridotitic garnets. Both lines are described in detail by Gurney and Zweistra [47].

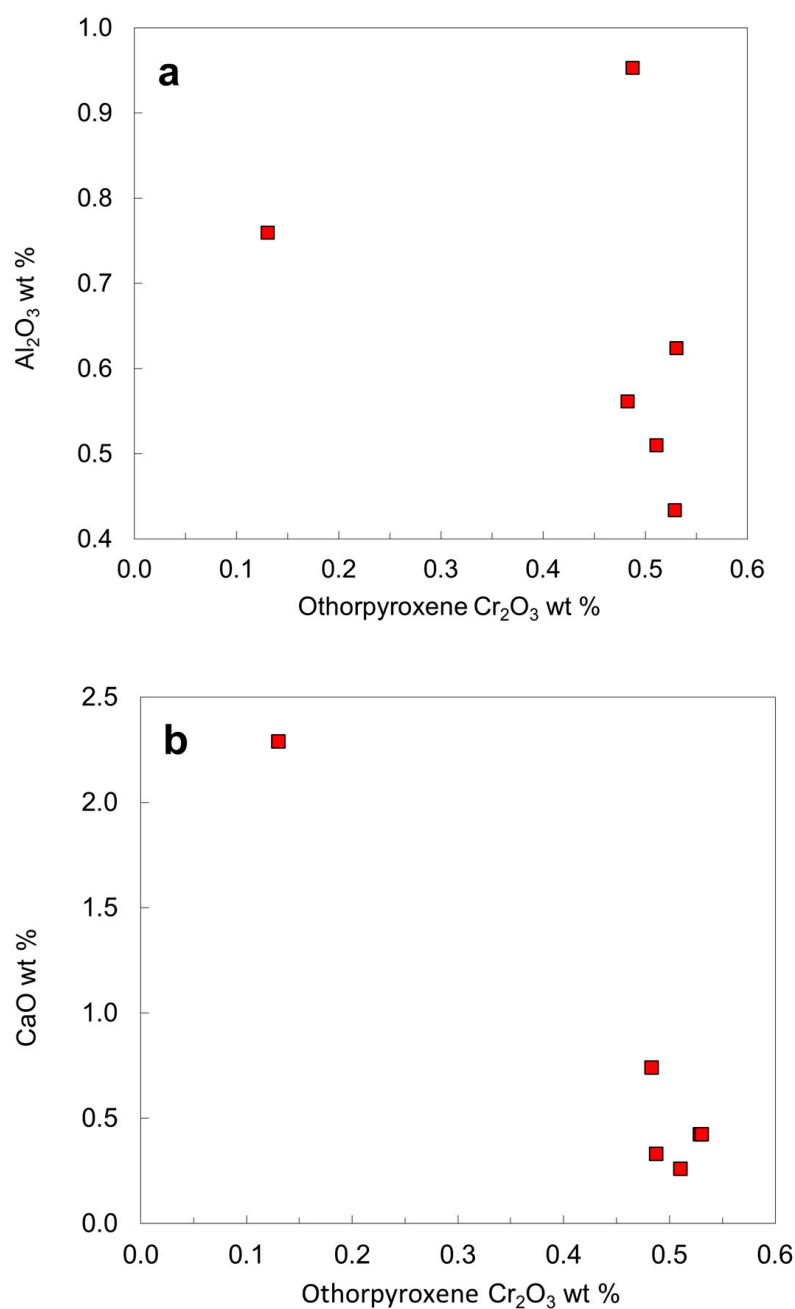


Figure 15. Compositional plots for orthopyroxene inclusions in diamond from the No. 50 kimberlite diatreme: (a) Cr₂O₃ versus Al₂O₃; (b) Cr₂O₃ versus CaO. All the harzburgitic orthopyroxenes are similar, but different from the websteritic orthopyroxene.

The olivine and orthopyroxene inclusions in the No 50 diamond are slightly enriched in iron compared with harzburgitic phases from worldwide sources [1], probably suggesting a relatively fertile character of harzburgitic mantle. In agreement with the expected olivine–orthopyroxene partitioning relationship in peridotite xenoliths [53], the peak of Mg # for the orthopyroxene is slightly higher than that of the olivine.

6.5. Chemical Compositions of Rare Mineral Inclusions

Carbonate. Carbonate inclusions in diamond are rare. The Ca-carbonate inclusion in sample LN50D11 (Figure 6b) was initially described as a silicate under optical microscope. The analyses using a EPMA procedure for silicate showed that the Ca-carbonate inclusion is mainly composed of CaCO₃ with minor MgCO₃ and FeCO₃. The loss of the Ca-carbonate

inclusion precludes further study of this interesting sample. A magnesite inclusion was found in a fracture of the diamond LN50D13 and coexists with a garnet grain. The coexistence of magnesite with garnet can be used to obtain an upper limit of oxygen fugacity from the reaction $6\text{MgCO}_3 + 22\text{Al}_2\text{SiO}_5 + 4\text{SiO}_2 = 2\text{Mg}_3\text{Al}_2\text{Si}_3\text{O}_{12} + 6\text{C} + 9\text{O}_2$ and a lower limit of oxygen fugacity in absence of periclase from the reaction $\text{MgCO}_3 = \text{MgO} + \text{C} + \text{O}_2$. Wang et al. [54] reported a magnesite inclusion in a diamond from the No. 50 kimberlite. Carbonate inclusions in diamonds from other kimberlites include Ca carbonate, magnesite, and dolomite [55–58].

Sulfides. Four primary inclusions and one secondary sulfide inclusion in diamond were exposed and analyzed. Representative chemical compositions of the sulfide inclusions are given in Table 6. Harris et al. [16] reported pyrrhotite with less than 1.0 wt. % of Co, Ni, Cu and Zn and pentlandite with 34–35 wt. % Ni in diamonds from the No. 50 kimberlite, but did not provide complete analyses. Some sulfide inclusions from other localities are given in Table 6 for comparison.

A sulfide inclusion in the diamond LN50D04 has a heterogeneous composition and shows Fe-rich, Ni-rich, and Cu-rich domains on X-ray map (Figure 7). The content of Cu could be high as 22 wt. % in some areas. The Σ cation/sulfur ratio of the most sulfide analyses is <1 (down to 0.800), indicating that the sulfide is predominantly pyrrhotite (R_{1-x}S). One analysis with Σ cation/sulfur = 1 may be troilite and one with a ratio of 1.047 may be pentlandite. Normalized to four atoms, some analyses have Σ cations slightly higher than, although close to, four, suggesting the existence of R_3S_4 minerals in the linnaeite group that includes violarite FeNi_2S_4 , daubreelite FeCr_2S_4 , greigite Fe_3S_4 , and carrollite $\text{Cu}(\text{Co},\text{Ni})_2\text{S}_4$. The sulfide inclusion in LN50D04 was initially analyzed at 20 kV and 10 nA. At these conditions, the Fe counts of Ni-rich domains could increase due to the fluorescence of Fe in the adjacent Fe-rich domain by Ni in the Ni-rich domain, thus producing excess cations relative to R_3S_4 phases. To examine this possibility, the inclusion was analyzed again at 10 kV and 20 nA condition. The effects of secondary fluorescence were not detected, and the calculated Σ cation/sulfur ratios remain similar. Chromium contents of the sulfide inclusion may be up to 0.85 wt. % (Figure 16d); K, Mn, Co, As, Se, Sb, Te, Ba and Bi in the sulfide are low or below the EPMA detection limit.

Sulfides from LN50D32 and LN50D37 have formulae near NiFe_2S_4 (Table 6). The sulfide in LN50D37 contains no Cu and its chemical variations are insignificant. This sulfide appears to be a solid solution between greigite ($\text{Fe}^{2+}\text{Fe}^{3+}_2\text{S}_4$) with polydymite ($\text{Ni}^{2+}\text{Ni}^{3+}_2\text{S}_4$), and/or violarite ($\text{Fe}^{2+}\text{Ni}^{3+}_2\text{S}_4$). The exact identity depends on knowing the valence of Ni and Fe, which could vary during the P-T history of the sulfide. Moreover, the composition of the LN50D37 sulfide is likely an average of a submicroscopic intergrowth. Sulfide from the LN50D42 belongs to pyrrhotite or pentlandite groups. Sulfide from the LN50D70 is located in a fracture and is secondary in origin (Table 6).

Bulanova et al. [59] used a proton microprobe to analyze sulfide inclusions in diamond. However, sulfide inclusions are compositionally heterogeneous and their sizes are usually small (mostly 20–50 μm in this work) and similar to the typical size of the proton beam spot on the sample (30–50 μm). Therefore, the large volumes (essentially entire inclusions) analyzed by the proton microprobe will give information on the average bulk composition of the original sulfide or melt.

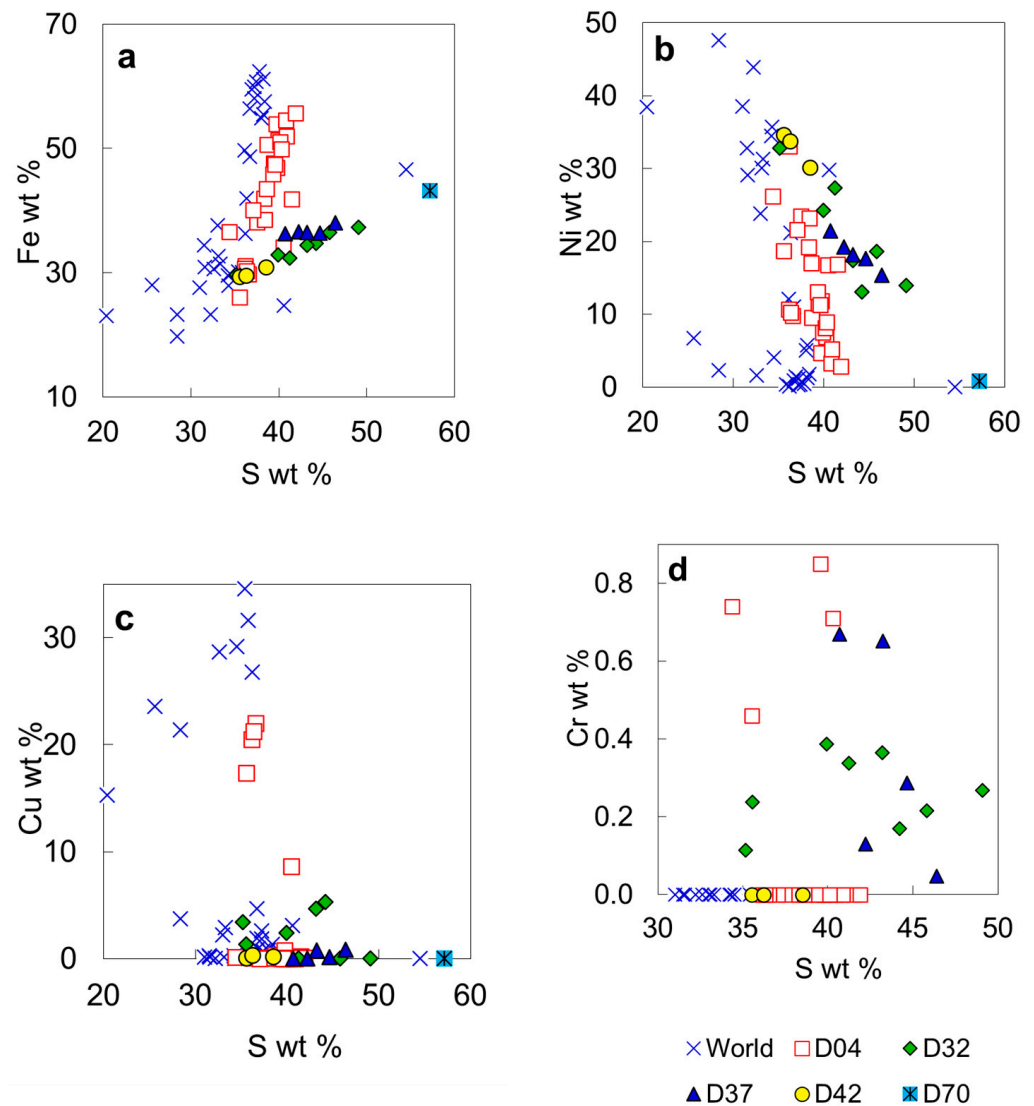


Figure 16. Compositional plots for sulfide inclusions in diamond from the No. 50 kimberlite diatreme: (a) S versus Fe; (b) S versus Ni; (c) S versus Cu; (d) S versus Cr.

Unknown hydrous silicate phase. The unknown silicate phase in sample LN50D67 (Figure 5c,d) is yellowish optically and has no fractures connected to the diamond surface. The inclusion has two compositional domains with one domain enriched in MgO and poor in SiO₂ relative to the other. The EPMA totals are low, from 85.9 to 90.2 wt. %, as is the case for serpentine, chlorite and humite (Table 7). The inclusion contains ~10 wt. % Al₂O₃, higher than most serpentine and lower than most chlorite, common alteration products of olivine. If H₂O is the only other component, the inclusion is a hydrous silicate in the system MgO-FeO-Al₂O₃-SiO₂-H₂O. There is another hydrous silicate inclusion reported in diamond from the same locality (Table 7). Hydrous dense silicate phases in system MgO-SiO₂-H₂O could be stable at very high pressure [60–62]. The unknown hydrous silicate phase is a hydrous Mg-Fe aluminosilicate, similar to Phase F (1.2MgO·1.8SiO₂·1.2H₂O) in MgO and H₂O if Al substitutes for Si and Mg simultaneously, or close to Phase D (MgO·SiO₂·H₂O) or Phase E (2.3MgO·1.25SiO₂·1.2H₂O) in SiO₂ and H₂O. The sample was lost during additional polishing, and no additional characterization could be undertaken.

Fe-rich phase. An Fe-rich phase in the diamond LN50D09 was discovered and analyzed for Fe, Co, Ni, Cu, Mn, Ba, Al, Si, and Cr, and the total oxides are approximately 80 wt. %, indicating the presence of other components (Table 8). Thus, the phase is neither native iron, wüstite, nor magnetite. Assuming the additional species is H₂O, the phase

is likely to be a hydrous iron oxide, such as goethite, FeOOH (Table 8). Other elements detected in the phase are Si (up to 3.8 wt. % SiO₂) and Al (up to 0.37 wt. % Al₂O₃) (Table 8). The paragenesis of this Fe-rich inclusion is unknown. The diamond host of this inclusion is cloudy and of poor quality. Although there is no visible fracture observed in the diamond host, the possibility of penetration of external components into the inside of diamond cannot be completely excluded. The inclusion was probably originally trapped as native iron, wüstite, or magnetite, and was later altered or modified by an external fluid. A similar Fe-dominant inclusion in diamond was described by Miao et al. [10] from the same locality (Table 8). Significant SiO₂ (0.8 wt. %) was also reported in a Fe-phase by Stachel et al. [57].

Table 7. Compositions of unknown hydrous phases in diamonds from the No. 50 kimberlite diatreme.

Mineral	LN50D67	LN50D67	Miao et al. [10]	Smyth & Kawamoto [61]		Burnley and Navrotsky [60]			
	Domain 1	Domain 2		Wadsleyite II		Phase D	Phase E	Phase F	
	Average	3 Analyses	3 Analyses	4 Analyses	1	2			
SiO ₂	47.27	41.29	65.81	SiO ₂	40.04	40.01	50.74	39.65	60.71
TiO ₂	0.01	0.01	0.06	TiO ₂	na	na	0.00	0.00	0.00
Al ₂ O ₃	10.01	10.42	0.91	Al ₂ O ₃	0.41	0.34	0.00	0.00	0.00
Cr ₂ O ₃	0.08	0.10	0.11	Cr ₂ O ₃	0.19	0.22	0.00	0.00	0.00
FeO	8.19	11.90	0.22	FeO	8.80	10.60	0.00	0.00	0.00
NiO	0.13	0.21	na	NiO	na	na	0.00	0.00	0.00
MnO	0.01	0.02	0.02	MnO	na	na	0.00	0.00	0.00
MgO	20.37	24.39	29.36	MgO	47.57	44.37	34.04	48.94	27.15
CaO	0.87	0.38	0.11	CaO	0.00	0.00	0.00	0.00	0.00
Σ	86.95	88.72	96.60	H ₂ O	2.99	4.46	15.21	11.41	12.14
H ₂ O	12.90	12.68	4.84	Σ	100.00	100.00	100.00	100.00	100.00
Σ	99.85	101.40	101.44						
Si	4.395	3.906	4.08	Si	0.975	0.980	1.000	1.250	1.800
Al	1.097	1.162	0.07	Al	0.012	0.010	0.000	0.000	0.000
Ti	0.001	0.000	0.00	Ti	0.000	0.000	0.000	0.000	0.000
Cr	0.006	0.008	0.01	Cr	0.004	0.004	0.000	0.000	0.000
Fe	0.637	0.942	0.01	Fe	0.179	0.217	0.000	0.000	0.000
Ni	0.008	0.013	0.00	Ni	0.000	0.000	0.000	0.000	0.000
Mn	0.000	0.001	0.00	Mn	0.000	0.000	0.000	0.000	0.000
Mg	2.822	3.439	2.71	Mg	1.726	1.620	1.000	2.300	1.200
Ca	0.087	0.039	0.01	Ca	0.000	0.000	0.000	0.000	0.000
Σcation	9.053	9.509	6.88	H	0.243	0.364	2.000	2.400	2.400
ΣO	14.000	14.000	11.00	Σcation	3.139	3.195	4.000	5.950	5.400
Mg #	81.6	78.5	99.58	ΣO	4.000	4.000	4.000	6.000	6.000

na: not analyzed. LN50D67: based on 6MgO.4SiO₂.4H₂O, normalized to 14 O excluding O in H₂O. Samples from Miao et al. [10]: based on 3MgO.4SiO₂.H₂O, normalized to 11 O excluding O in H₂O.

Table 8. Compositions of an unknown Fe-rich phase in diamond from the No. 50 kimberlite diatreme.

Analysis	LN50D09 (Goethite or Limonite?)						Miao et al. [10]		
	a1	a2	b1	b2	b3	b4	Average	Goethite (?)	Ideal Goethite
Al ₂ O ₃	0.11	0.37	0.26	0.10	0.35	0.18	0.25	0.54	0.00
SiO ₂	3.77	3.53	3.66	1.39	3.64	3.63	3.27	na	0.00
Cr ₂ O ₃	0.02	0.03	0.12	0.00	0.04	0.09	0.05	na	0.00
MnO	0.00	0.00	0.00	0.00	0.00	0.00	0.00	0.09	0.00
Fe ₂ O ₃	80.68	81.75	80.54	78.86	82.04	79.92	80.63	85.30	87.98
CoO	0.00	0.00	0.00	0.00	0.00	0.00	0.00	na	0.00
NiO	0.10	0.02	0.08	0.11	0.04	0.09	0.07	na	0.00
CuO	0.00	0.00	0.06	0.06	0.08	0.33	0.10	na	0.00
BaO	0.14	0.08	0.14	0.02	0.07	0.10	0.09	na	0.00
H ₂ O	15.19	14.21	15.14	19.47	13.74	15.66	15.53	14.07	12.02
Σ	100.00	100.00	100.00	100.00	100.00	100.00	100.00	100.00	100.00
	Oxygen normalized to 3								
Al	0.004	0.013	0.009	0.004	0.012	0.007	0.009	0.020	0.000
Si	0.114	0.106	0.111	0.045	0.109	0.111	0.100	0.000	0.000
Cr	0.000	0.001	0.003	0.000	0.001	0.002	0.001	0.000	0.000
Mn	0.000	0.000	0.000	0.000	0.000	0.000	0.000	0.002	0.000
Fe ³⁺	1.841	1.844	1.837	1.933	1.840	1.836	1.853	1.979	2.000
Co	0.000	0.000	0.000	0.000	0.000	0.000	0.000	0.000	0.000
Ni	0.002	0.001	0.002	0.003	0.001	0.002	0.002	0.000	0.000
Cu	0.000	0.000	0.001	0.001	0.002	0.008	0.002	0.000	0.000
Ba	0.002	0.001	0.002	0.000	0.001	0.001	0.001	0.000	0.000
Σcation	1.963	1.965	1.965	1.986	1.965	1.967	1.968	2.001	2.000
Σcharge	6.000	6.000	6.000	6.000	6.000	6.000	6.000	6.000	6.000
H ₂ O molecule	1.265	1.183	1.261	1.621	1.144	1.304	1.293	1.172	1.000

H₂O by difference; na: not analyzed.

6.6. Origin of Sulfide Inclusions in Diamond

Sulfide inclusions in diamond are common [1,63,64] and may occur as discrete crystals [65]. Primary sulfide inclusions in diamonds have been shielded from the interaction with the outside environment. Therefore, such sulfide inclusions provide information on the primary compositions of mantle sulfide, the distribution and abundance of chalcophile elements in the mantle, and the formation environment of the host diamond [66,67]. Sulfide inclusions in diamonds are associated with either peridotitic or eclogitic assemblages [59,65]. On the base of the inclusion assemblage, the sulfide inclusion in the diamond LN50D04, which contains chromite and olivine, belongs to the peridotitic suite. In Siberian, peridotitic sulfides in diamond show significantly higher Ni and Cu contents than eclogitic sulfides [59]. The boundary between peridotitic and eclogitic sulfide inclusions is 8 wt. % Ni [65], or 12 wt. % Ni, or it is transitional [59]. Experimental studies on Ni/Fe exchange between olivine and monosulfide solid solution [68–70] indicate that, for peridotitic olivine with Fo88–Fo94 and 2500–3500 ppm Ni, the coexisting monosulfide solid solution will contain 30–55 mol % NiS (25–35 wt. % Ni). The sulfide inclusion in the diamond LN50D42 has a Ni content of ~30 wt. % and was probably in equilibrium with mantle olivine. If sulfide were the only inclusion in diamond, it may be difficult to determine which assemblage a sulfide inclusion might belong to based on Ni content. For example, the peridotitic sulfide in the diamond LN50D04 have Ni content from 6 to 34.6 wt. % (Figure 16b), whereas an eclogitic sulfide in an omphacite- and coesite-bearing diamond contains >11 wt. % Ni [59]. Deines and Harris [71] demonstrated that assignment of Ni-rich monosulfide to the peridotitic paragenesis is ambiguous if there is no further evidence from coexisting silicate inclusions.

Iron–nickel–copper sulfides are the most abundant primary sulfide inclusions in diamond [53,59,72]. Based on the stability of diamond (1500 K at 50 kbar [73]) and silicate assemblages in diamond, sulfide was trapped at around 1000–1200 °C. At these temperatures, monosulfide solid solution and sulfide melt coexist over a wide range of compositions [74,75]. Therefore, iron–nickel–copper sulfides in diamonds might be trapped as droplets of primary, immiscible sulfide melt, such as those from silicate megacrysts in basalt [76], or as crystals of monosulfide solid solution which then exsolved to different sulfide after subsolidus re-equilibration [1,2,27,63,64,77–80] (. Element partitioning between sulfide melt and monosulfide crystal at mantle conditions is controlled by composition, temperature, and pressure. The effect of melt composition and temperature on element partitioning between sulfide melts and monosulfide crystals suggest that Cu and Ni are slightly concentrated in residual melt during fractional crystallization at 1000–1100 °C [81]. Therefore, monosulfide solid solution crystallized from melts would contain low Ni and Cu, whereas the residual melts would be enriched in Ni and Cu. According to Bulanova et al. [59], peridotitic sulfide inclusions with Cu > 3 wt. % and Ni > 17 wt. % may represent entrapped melts. The bulk composition of each sulfide inclusion in diamond from the No. 50 diatreme likely has low Cu content (<3 wt. %), although a few analyses of the sulfide inclusions have higher Cu contents (Table 6). The Ni contents of the sulfide inclusions are widespread, from ~3 to >30 wt. % (Table 6). The Cu and Ni contents appear to suggest that the most sulfide inclusions were trapped as monosulfide crystals and some may be trapped as melts.

6.7. Source Rocks, Metasomatism, and Diamond Formation

The mineral inclusions examined in this study belong to harzburgitic and lherzolitic suites. Lherzolitic and harzburgitic inclusions can be recognized on the base of chemical compositions of garnet. For example, on a CaO versus Cr₂O₃ diagram for garnet (Figure 14), a solid line distinguishes lherzolitic garnet field (lower right side) from harzburgitic garnet field (upper left side) [46]. The compositions of most garnet inclusions from the No. 50 diatreme falls within the harzburgitic field, indicating that the main source rock of the diamonds is harzburgitic, while the lherzolitic assemblage is minor. The dominant harzburgitic source is consistent with the types of mineral inclusions recovered in diamond.

The present study shows that there are abundant olivine, chromite, orthopyroxene and garnet inclusions in diamond, but rare clinopyroxene inclusions. The harzburgitic mantle likely formed by earlier extensive partial melting, whereas the lherzolitic mantle may have experienced a smaller degree of partial melting because of the high Mg # of the olivine.

Although they come from a harzburgitic diamond source, olivine inclusions are slightly variable in composition. For example, the olivine inclusions have a somewhat lower Mg # (peak at 93, Figure 9a) than similar harzburgitic inclusions worldwide (Mg # peak at 94, [1]), indicating that the harzburgitic mantle source was either chemically less depleted than in most other cratons or had been re-enriched in iron. Another feature of olivine inclusions is their higher Ni content. The NiO content of the olivine inclusions vary from 0.25 to 0.45 wt. % with a peak around 0.40 wt. % (Table 2; Figure 9b), higher than that for the olivine inclusions worldwide (0.36 wt. %, [24]). One olivine inclusion contains as high as 0.8 wt. % NiO (Table 2). In addition, some chromite inclusions in the diamond from the No. 50 kimberlite contain up to 0.79 wt. % TiO₂, higher than the maximum TiO₂ content (0.65 wt. %) of chromite inclusions in diamond worldwide. The above features, plus the existence of carbonate inclusions and the possible presence of hydrous silicate phases in diamond, imply a metasomatic enrichment event in the source region of diamond beneath the North China craton. We suggest that the diamond from the No. 50 kimberlite diatreme likely formed by growth under metasomatic conditions with the presence of a fluid.

Funding: This study was supported by funding from NSF (EAR 93-15918, 94-58368 and 97-25566 to YZ, EAR 91-17772 and 95-26596 to EJE), NWT Geology Division of DIAND of the Government of Canada, the University of Michigan, and the Geological Society of America. The electron microprobe analyzer used in this work was acquired under Grant # EAR-82-12764 from the National Science Foundation.

Acknowledgments: The diamond samples were provided by or purchased from the Sixth Geological Exploration Team of Liaoning Province. The field trip was sponsored by the Institute of Mineral Resources of Chinese Academy of Geological Sciences and the Liaoning Sixth Geological Team. Yunhui Huang, Shuying Qin, Zhuguo Han, Yawen Cao, Ruishan Liu, Jize Lin, Qing Miao, Liping Wang, Weixin Wang, and Xianfeng Fu are thanked for providing samples or for assistance for facilitating the field trip. This study was supervised by Eric J. Essene and Youxue Zhang in Department of Geological Sciences at the University of Michigan. Two anonymous reviewers are thanked for their helpful and constructive comments.

Conflicts of Interest: The authors declare no conflict of interest.

References

1. Meyer, H.O.A. Inclusions in diamonds. In *Mantle Xenoliths*; Nixon, P.H., Ed.; John Wiley and Sons: Hoboken, NJ, USA, 1987; pp. 501–522.
2. Moore, R.O.; Gurney, J.J. Inclusions in diamond from the Monastery kimberlite, South Africa. In *Kimberlites and Related Rocks Volume 2: Their Mantle/Crustal Setting, Diamonds and Diamond Exploration, Proceedings of the Fourth International Kimberlite Conference, Perth, Australia, 11–15 August 1986*; Ross, J., Jaques, A.L., Ferguson, J., Green, D.H., O'Reilly, S.Y., Danchin, R.Y., Janse, A.J.A., Eds.; Geological Society of Australia Special Publication 14 (2); Geological Society of Australia: Hornsby, Australia, 1989; pp. 1029–1041.
3. Huang, Y.; Qin, S.; Zhou, X.; Deng, C.; Zhao, D.; Yang, J.; Guo, Y.; Gao, Y.; Li, G. *Kimberlites and Diamonds in the North China Craton*; Geological Publishing House: Beijing, China, 1992; 206p. (In Chinese)
4. Leung, I.S. The discovery of calcite inclusion in natural diamond and its implications on the genesis of diamond, kimberlite and carbonatite. In *Geological Society of America 97th Annual Meeting Abstract and Programs, Proceedings of the Geological Society of America 97th Annual Meeting, Reno, NV, USA, 5–8 November 1984*; Geological Society of America: Boulder, CO, USA, 1984; Volume 16, p. 574.
5. Leung, I.S. Silicon carbide cluster entrapped in a diamond from Fuxian, China. *Am. Mineral.* **1990**, *75*, 1110–1119.
6. Leung, I.S. Metasomatized olivine, garnet and diopside entrapped in diamonds from Fuxian. *Eos* **1994**, *74*, 192.
7. Zhang, A.; Meyer, H.O.A. Inclusions in diamonds from Chinese kimberlites. In *Extended Abstracts of the 28th IGC Workshop on Diamonds*; The Congress: Washington, DC, USA, 1989; pp. 1–3.
8. Deng, C.; Huang, Y.; Zhao, D. Mineral inclusions in the Chinese diamonds. In *Extended Abstracts of the 15th IMA General Meeting*; International Mineralogical Association: Aubièrre, France, 1990; Volume 1, pp. 487–488.
9. Dong, Z. Mineral inclusions in diamonds. *Mineral. Petrol.* **1991**, *11*, 64–71, (In Chinese with English Abstract).

10. Miao, Q.; Liu, G.; Lu, Q.; Wang, X.; Zheng, C. New discovery of complicated inclusions in diamonds and their origin. *Geol. Sci. Technol. Inf.* **1991**, *10*, 117–123. (In Chinese)
11. Wang, A.; Wang, W.; Zhang, A. Microstructural variations of a pyrope inclusion in diamond, as revealed by a micro-Raman spectroscopic study. *Can. Mineral.* **1991**, *29*, 517–524.
12. Wang, A.; Dhameincourt, P.; Meyer, H.O.A.; Guo, L.; Zhang, A. A carbon-rich multiphase inclusion in a Chinese diamond and its geochemical implications. *Contrib. Mineral. Petrol.* **1994**, *117*, 15–24. [[CrossRef](#)]
13. Chen, F.; Wang, M.; Wang, S.; Ding, Z.; Guo, J.; Wang, Z.; Lei, P.; Zhang, Y. First discovery of High-Cu and high-Cl inclusions in diamond. *Kexue Tongbao (Chin. Sci. Bull.)* **1992**, *37*, 1782–1784. (In Chinese)
14. Miao, Q. The characteristic of diamonds from Toudaogou placer deposit, Southern Liaoning, China. *Collect. Mineral. Petrol.* **1992**, *8*, 25–32. (In Chinese with English Abstract)
15. Zhao, D.; Deng, C.; Yang, J. Diamonds from East China: Morphology and inclusions. *Eos* **1993**, *74*, 168.
16. Harris, J.W.; Duncan, D.J.; Zhang, F.; Miao, Q.; Zhu, Y. The physical characteristics and syngenetic inclusion geochemistry of diamonds from Pipe 50, Liaoning Province, People's Republic of China. In *Diamonds: Characterization, Genesis and Exploration, Proceedings of the Fifth International Kimberlite Conference, Araxa, Brazil, 18 June–4 July 1991*; Meyer, H.O.A., Leonardos, O.H., Eds.; CPRM-Special Publication; Companhia de Pesquisa de Recursos Minerais: Rio de Janeiro, Brazil, 1994; Volume 2, pp. 106–115.
17. Meyer, H.O.A.; Zhang, A.; Milledge, H.J.; Mendelsohn, M.J. Diamonds and inclusions in diamonds from Chinese kimberlites. In *Diamonds: Characterization, Genesis and Exploration, Proceedings of the Fifth International Kimberlite Conference, Araxa, Brazil, 18 June–4 July 1991*; Meyer, H.O.A., Leonardos, O.H., Eds.; CPRM-Special Publication; Companhia de Pesquisa de Recursos Minerais: Rio de Janeiro, Brazil, 1994; Volume 2, pp. 98–105.
18. Wang, Z.; Guo, G. Characteristics of inclusions from diamonds in No. 50 pipe at Wafangdian, South Liaoning. *Liaoning Geol.* **1994**, 263–274. (In Chinese with English Abstract)
19. Gorshkov, A.I.; Bao, Y.; Bershov, L.V.; Ryabchikov, I.D.; Sivtsov, A.V.; Lapina, M.I. Inclusions in diamond from the Liaoning deposit (China) and their genetic meaning. *Geochem. Int.* **1997**, *35*, 51–57.
20. Gorshkov, A.I.; Bao, Y.; Bershov, L.V.; Ryabchikov, I.D.; Sivtsov, A.V.; Lapina, M.I. Inclusions of native metals and other minerals in diamond from kimberlite pipe 50, Liaoning, China. *Geochem. Int.* **1997**, *35*, 695–703.
21. Zhao, D. Electron Probe Microanalysis and Microscopy: Focused Electron Beam Techniques and Applications in Characterization of Mineral Inclusions in Diamond. *Microsc. Microanal.* **2015**, *21* (Suppl. 3), 1319–1320. [[CrossRef](#)]
22. Bulanova, G.P. The formation of diamond. *J. Geochem. Explor.* **1995**, *53*, 1–23. [[CrossRef](#)]
23. Kopylova, M.G.; Gurney, J.J.; Daniels, L.R.M. Mineral inclusions in diamonds from the River Ranch kimberlite, Zimbabwe. *Contrib. Mineral. Petrol.* **1997**, *129*, 366–384. [[CrossRef](#)]
24. Stachel, T.; Harris, J.W. Syngenetic inclusions in diamond from the Birim field (Ghana)—A deep peridotitic profile with a history of depletion and re-enrichment. *Contrib. Mineral. Petrol.* **1997**, *127*, 336–352. [[CrossRef](#)]
25. Zhao, D. Kimberlite, Diamond and Mantle Xenolith from Northwest Territories, Canada and North China. Ph.D. Thesis, University of Michigan, Ann Arbor, MI, USA, 1998.
26. Zhao, D.; Zhang, Y.; Essene, E.J. Electron Probe Microanalysis and Microscopy: Principles and Applications in Characterization of Mineral Inclusions in Chromite from Diamond Deposit. *Ore Geol. Rev.* **2015**, *65*, 733–748. [[CrossRef](#)]
27. Harris, J.W. Diamond geology. In *The Properties of Natural and Synthetic Diamond*; Field, J.E., Ed.; Academic Press: London, UK, 1992; pp. 345–393.
28. Harris, J.W. Black material on mineral inclusions and in internal fracture planes in diamond. *Contrib. Mineral. Petrol.* **1972**, *129*, 22–33. [[CrossRef](#)]
29. Gorshkov, A.I.; Titkov, S.V.; Sivtsov, A.V.; Bershov, L.V.; Marfunin, A.S. The first finds of native Cr, Ni, and Fe in carbonado from the diamond deposits of Yakutia. *Geochem. Int.* **1996**, *33*, 59–63.
30. Foster, N.F.; Wozniakiewicz, P.J.; Price, M.C.; Kearsley, A.T.; Burchell, M.J. Identification by Raman spectroscopy of Mg–Fe content of olivine samples after impact at 6 km s⁻¹ onto aluminium foil and aerogel: In the laboratory and in Wild-2 cometary samples. *Geochim. Cosmochim. Acta* **2013**, *121*, 1–14. [[CrossRef](#)]
31. Kleppe, A.K.; Jephcoat, A.P.; Smyth, J.R. High-pressure Raman spectroscopic studies of hydrous wadsleyite II. *Am. Mineral.* **2006**, *91*, 1102–1109. [[CrossRef](#)]
32. Sobolev, N.V.; Logvinova, A.M.; Zedgenizov, D.A.; Seryotkin, Y.V.; Yefimova, E.S.; Floss, C.; Taylor, L.A. Mineral inclusions in microdiamonds and macrodiamonds from kimberlites of Yakutia: A comparative study. *Lithos* **2004**, *77*, 225–242. [[CrossRef](#)]
33. Sobolev, N.V.; Logvinova, A.M.; Zedgenizov, D.A.; Pokhilenko, N.P.; Kuzmin, D.V.; Sobolev, A.V. Olivine inclusions in Siberian diamonds: High precision approach to minor elements. *Eur. J. Mineral.* **2008**, *20*, 305–315. [[CrossRef](#)]
34. Griffin, W.L.; Cousens, D.R.; Ryan, C.G.; Sie, S.H.; Suter, G.F. Ni in chrome pyrope garnets: A new geothermometer. *Contrib. Mineral. Petrol.* **1989**, *103*, 199–202. [[CrossRef](#)]
35. Ryan, C.G.; Griffin, W.L.; Pearson, N.J. Garnet geotherms—Pressure-temperature data from Cr-pyrope garnet xenocrysts in volcanic rocks. *J. Geophys. Res.* **1996**, *101*, 5611–5625. [[CrossRef](#)]
36. Ryabchikov, I.D.; Green, D.H.; Wall, V.; Brey, G.P. The oxidation state of carbon in the reduced velocity zone. *Geochem. Int.* **1981**, *18*, 148–158.
37. Smith, J.V.; Steele, I.M. Lunar mineralogy; a heavenly detective story: Part II. *Am. Mineral.* **1976**, *61*, 1059–1116.

38. Li, J.-P.; O'Neill, H.S.C.; Seifert, F. Subsolidus phase relations in the system MgO-SiO₂-Cr-O in equilibrium with metallic Cr, and their significance for the petrochemistry of chromium. *J. Petrol.* **1995**, *36*, 107–132. [[CrossRef](#)]
39. Sutton, S.R.; Bajt, S.; Rivers, M.L.; Smith, J.V.; Blanchard, D.; Black, D. X-ray microprobe determination of chromium oxidation state in olivine from lunar basalt and kimberlitic diamonds. In *Abstracts of Papers Submitted to the Lunar and Planetary Science Conference*; American Geophysical Union: Washington, DC, USA, 1993; Volume 24, pp. 1383–1384.
40. Köhler, T.P.; Brey, G.P. Calcium exchange between olivine and clinopyroxene calibrated as a geothermobarometer for natural peridotites from 2–60 kb with applications. *Geochim. Cosmochim. Acta* **1990**, *54*, 2375–2388. [[CrossRef](#)]
41. Lee, D.-C.; Halliday, A.N.; Davies, G.R.; Essene, E.J.; Fitton, J.G.; Temdjim, R. Melt enrichment of shallow depleted mantle: A detailed petrological, trace element and isotopic study of mantle derived xenoliths and megacrysts from the Cameroon line. *J. Petrol.* **1996**, *37*, 415–441. [[CrossRef](#)]
42. Woodland, A.B.; O'Neill, H.S.C. Synthesis and stability of Fe₃²⁺Fe₂³⁺Si₃O₁₂ garnet and phase relations with Fe₃Al₂Si₃O₁₂—Fe₃²⁺Fe₂³⁺Si₃O₁₂ solutions. *Am. Mineral.* **1993**, *78*, 1002–1015.
43. Brey, G.; Doroshev, A.; Kogarko, L. The join pyrope-knorringite: Experimental constraints for a new geothermobarometer for coexisting garnet and spinel. In *Extended Abstracts of the Fifth International Kimberlite Conference*; CPRM-Special Publication, 2/91; Meyer, H.O.A., Leonardos, O.H., Eds.; Companhia de Pesquisa de Recursos Minerais: Araxa, Brazil, 1991; pp. 26–28.
44. Gurney, J.J.; Harris, J.W.; Rickard, R.S. Minerals associated with diamonds from the Roberts Victor Mine. In *Kimberlites II: Their Mantle and Crust-Mantle Relationships, Proceedings of the Third International Kimberlite Conference, Clermont-Ferrand, France, September 1982*; Kornprobst, J., Ed.; Developments in Petrology, 11B; Elsevier: Amsterdam, The Netherlands, 1984; pp. 25–32.
45. Wilding, M.C.; Harte, B.; Harris, J.W. Inclusion chemistry, carbon isotopes and nitrogen distribution in Bultfontein diamonds: The evolution of natural diamond growth conditions. In *Extended Abstracts of the Fifth International Kimberlite Conference*; CPRM-Special Publication, 2/91; Meyer, H.O.A., Leonardos, O.H., Eds.; Companhia de Pesquisa de Recursos Minerais: Araxa, Brazil, 1991; p. 459.
46. Sobolev, N.V.; Lavrent'ev, Y.G.; Pokhilenko, N.P.; Usova, L.V. Chrome-rich garnets from the kimberlites of Yakutia and their paragenesis. *Contrib. Mineral. Petrol.* **1973**, *40*, 39–52. [[CrossRef](#)]
47. Gurney, J.J.; Zweistra, P. The interpretation of the major element compositions of mantle minerals in diamond exploration. *J. Geochem. Explor.* **1995**, *53*, 293–309. [[CrossRef](#)]
48. Ringwood, A.E. *Composition and Petrology of the Earth's Upper Mantle*; McGraw-Hill: London, UK, 1975.
49. Moore, R.O.; Gurney, J.J. Pyroxene solid solution in garnets included in diamonds. *Nature* **1985**, *318*, 553–555. [[CrossRef](#)]
50. Irifune, T. An experimental investigation of the pyroxene garnet transformation in a pyrolite composition and its bearing on the constitution of the mantle. *Phys. Earth Planet. Inter.* **1987**, *45*, 324–336. [[CrossRef](#)]
51. Wang, L.; Essene, E.J.; Zhang, Y. Mineral inclusions in pyrope crystals from Garnet Ridge, Arizona, USA: Implications for processes in the upper mantle. *Contrib. Mineral. Petrol.* **1999**, *135*, 164–178. [[CrossRef](#)]
52. Tsai, H.M.; Meyer, H.O.; Mozeau, J.; Milledge, H.J. Mineral inclusions in diamond: Premier, Jagersfontein and Finch kimberlites, South Africa, and Williamson Mine, Tanzania. In *Kimberlites, Diatremes and Diamonds: Their Geology and Petrology and Geochemistry*; Boyd, F.R., Meyer, H.O.A., Eds.; American Geophysical Union: Washington, DC, USA, 1979; pp. 16–26.
53. Gurney, J.J.; Harris, J.W.; Rickard, R.S. Silicate and oxide inclusions in diamonds from the Finsch kimberlite pipe. In *Kimberlites, Diatremes and Diamonds: Their Geology and Petrology and Geochemistry*; Boyd, F.R., Meyer, H.O.A., Eds.; American Geophysical Union: Washington, DC, USA, 1979; pp. 1–15.
54. Wang, A.; Pasteris, J.D.; Meyer, H.O.A.; Deleduboi, M.L. Magnesite-bearing inclusion assemblage in natural diamond. *Earth Planet. Sci. Lett.* **1996**, *141*, 293–306. [[CrossRef](#)]
55. Meyer, H.O.A.; McCallum, M.E. Mineral inclusions in diamonds from the Sloan kimberlites, Colorado. *J. Geol.* **1986**, *94*, 600–612. [[CrossRef](#)]
56. Phillips, D.; Harris, J.W. Geothermobarometry of diamond inclusions from the De Beers Pool Mines, Kimberley, South Africa. In *Extended Abstracts of the Sixth International Kimberlite Conference*; Sobolev, N.V., Ed.; United Institute of Geology, Geophysics and Mineralogy, Siberian Branch of Russian Academy of Sciences: Novosibirsk, Russia, 1995; pp. 441–443.
57. Stachel, T.; Harris, J.W.; Brey, G.P. Rare and unusual mineral inclusions in diamonds from Mwadui, Tanzania. *Contrib. Mineral. Petrol.* **1998**, *132*, 34–47. [[CrossRef](#)]
58. Logvinova, A.M.; Wirth, R.; Zedgenizov, D.A.; Taylor, L.A. Carbonate–Silicate–Sulfide Polyphase Inclusion in Diamond from the Komsomolskaya Kimberlite Pipe, Yakutia. *Geochem. Int.* **2018**, *56*, 283–291. [[CrossRef](#)]
59. Bulanova, G.P.; Griffin, W.L.; Ryan, C.G.; Shestakova, O.Y.; Barnes, S.J. Trace elements in sulfide inclusions from Yakutian diamonds. *Contrib. Mineral. Petrol.* **1996**, *124*, 111–125. [[CrossRef](#)]
60. Burnley, P.C.; Navrotsky, A. Synthesis of high-pressure hydrous magnesium silicates: Observations and analysis. *Am. Mineral.* **1996**, *81*, 317–326. [[CrossRef](#)]
61. Smyth, J.R.; Kawamoto, T. Wadsleyite II: A new high pressure hydrous phase in the peridotite-H₂O system. *Earth Planet. Sci. Lett.* **1997**, *146*, E9–E16. [[CrossRef](#)]
62. Shieh, S.R.; Mao, H.K.; Konzett, J.; Hemley, R.J. In-situ high pressure X-ray diffraction of phase E to 15 GPa. *Am. Mineral.* **2000**, *85*, 765–769. [[CrossRef](#)]
63. Sharp, W.E. Pyrrhotite: A common inclusion in South Africa diamonds. *Nature* **1966**, *211*, 402–403. [[CrossRef](#)]

64. Gurney, J.J. Diamonds. In *Kimberlites and Related Rocks Volume 2: Their Mantle/Crustal Setting, Diamonds and Diamond Exploration, Proceedings of the Fourth International Kimberlite Conference, Perth, Australia, 11–15 August 1986*; Ross, J., Jaques, A.L., Ferguson, J., Green, D.H., O'Reilly, S.Y., Danchin, R.Y., Janse, A.J.A., Eds.; Geological Society of Australia Special Publication 14 (2); Geological Society of Australia: Hornsby, Australia, 1989; pp. 935–965.
65. Yefimova, E.S.; Sobolev, N.V.; Pospelova, L.N. Sulfide inclusions in diamond and specific features of their paragenesis. *Zap. Vsesoyuznogo Mineral. Obs.* **1983**, *112*, 300–310. (In Russian)
66. Zhimulev, E.I.; Chepurov, A.I.; Sinyakova, E.F.; Sonin, V.M.; Chepurov, A.A.; Pokhilenko, N.P. Diamond crystallization in the Fe-Co-S-C and Fe-Ni-S-C systems and the role of sulfide-metal melts in the genesis of diamond. *Geochem. Int.* **2012**, *50*, 205–216. [[CrossRef](#)]
67. Palyanov, Y.N.; Borzdov, Y.M.; Bataleva, Y.V.; Kupriyanov, I.N. Diamond formation during sulfidation of metal–carbon melts. *Diam. Relat. Mater.* **2021**, *120*, 108660. [[CrossRef](#)]
68. Fleet, M.E.; MacRae, N.D.; Herzberg, C.T. Partition of nickel between olivine and sulfide: A test for immiscible liquids. *Contrib. Mineral. Petrol.* **1977**, *65*, 191–197. [[CrossRef](#)]
69. Fleet, M.E.; MacRae, N.D. Partition of Ni between olivine and sulfide: The effect of temperature, fO_2 and fS_2 . *Contrib. to Mineral. Petrol.* **1987**, *95*, 75–81. [[CrossRef](#)]
70. Fleet, M.E.; MacRae, N.D. Partition of nickel between olivine and sulfide: Equilibria with sulfide-oxide liquids. *Contrib. Mineral. Petrol.* **1988**, *100*, 462–469. [[CrossRef](#)]
71. Deines, P.; Harris, J.W. Sulfide inclusion chemistry and carbon isotopes of African diamonds. *Geochim. Cosmochim. Acta* **1995**, *59*, 3173–3188. [[CrossRef](#)]
72. Harris, J.W.; Gurney, J.J. Inclusions in diamond. In *The Properties of Diamond*; Field, J.E., Ed.; Academic Press: London, UK, 1979; pp. 555–591.
73. Kennedy, C.S.; Kennedy, G.C. The equilibrium boundary between graphite and diamond. *J. Geophys. Res.* **1976**, *81*, 2467–2470. [[CrossRef](#)]
74. Craig, J.R.; Kullerud, G. Phase relations in the Cu-Fe-Ni-S system and their application to magmatic ore deposits. *Econ. Geol. Monogr.* **1969**, *4*, 344–358.
75. Sugaki, A.; Kitakaze, A. High form of pentlandite and its thermal stability. *Am. Mineral.* **1998**, *83*, 133–140. [[CrossRef](#)]
76. Andersen, T.; Griffin, W.L.; O'Reilly, S.Y. Primary sulphide melt inclusions in mantle-derived megacrysts and pyroxenites. *Lithos* **1987**, *20*, 279–294. [[CrossRef](#)]
77. Meyer, H.O.A.; Svisero, D.P. Mineral inclusions in Brazilian diamonds. *Phys. Chem. Earth* **1975**, *9*, 785–795. [[CrossRef](#)]
78. Otter, M.L.; Gurney, J.J. Inclusions in diamonds from the Sloan diatremes, Colorado-Wyoming State Line kimberlite district, North America. In *Kimberlites and Related Rocks Volume 2: Their Mantle/Crustal Setting, Diamonds and Diamond Exploration, Proceedings of the Fourth International Kimberlite Conference, Perth, Australia, 11–15 August 1986*; Ross, J., Jaques, A.L., Ferguson, J., Green, D.H., O'Reilly, S.Y., Danchin, R.Y., Janse, A.J.A., Eds.; Geological Society of Australia Special Publication 14 (2); Geological Society of Australia: Hornsby, Australia, 1989; pp. 1042–1053.
79. Sobolev, N.V.; Kaminsky, F.V.; Griffin, W.L.; Yefimova, E.S.; Win, T.T.; Ryan, C.G.; Botkunov, A.I. Mineral inclusions in diamonds from the Sputnik kimberlite pipe, Yakutia. *Lithos* **1997**, *39*, 135–157. [[CrossRef](#)]
80. Taylor, L.A.; Liu, Y. Sulfide inclusions in diamonds: Not monosulfide solid solution. *Russ. Geol. Geophys.* **2009**, *50*, 1201–1211. [[CrossRef](#)]
81. Li, C.; Barnes, S.-J.; Makovicky, E.; Rose-Hansen, J.; Makovicky, M. Partitioning of nickel, copper, iridium, rhenium, platinum, and palladium between monosulfide solid solution and sulfide liquid: Effects of composition and temperature. *Geochim. Cosmochim. Acta* **1996**, *60*, 1231–1238. [[CrossRef](#)]